CrystEngComm

HIGHLIGHT

View Article Online
View Journal | View Issue

Cite this: *CrystEngComm*, 2017, **19**, 3867

Hydrothermal synthesis of strontium titanate: thermodynamic considerations, morphology control and crystallisation mechanisms

Giovanna Canu and Vincenzo Buscaglia *

This article highlights the recent developments on the hydrothermal and solvothermal synthesis of strontium titanate ($SrTiO_3$), considered as a model system, by reviewing the literature of the last 10–15 years. The most significant advantage of these solution-mediated crystallisation methods is the effective control of particle composition, size and morphology by varying some physical and chemical parameters such as temperature, concentration, pH and solvent composition, as well as using different precursors and mineralisers, and moreover, adding growth modifiers like polar organic molecules and hydrophilic polymers. Thus, the synthesis process can be designed to obtain pure and doped materials with superior functional and photocatalytic properties, including monodispersed nanoparticles, platelets, wires, porous particles, mesocrystals and heterostructures. The hydrothermal crystallisation mechanisms are critically discussed, considering both the thermodynamic and kinetic aspects. In particular, the nature and morphology of the solid titanium precursor has a significant impact on the hydrothermal crystallisation as in many cases the formation of $SrTiO_3$ occurs on the precursor surface. The dissolution of the precursor and the nucleation and growth of the perovskite are coupled together over rather short distances, and the coupling is mediated by the solid/liquid interfaces. The morphology of strontium titanate is thus determined by the precursor/perovskite crystallographic matching, the surface density of nuclei and the rate-controlling process. Differently, crystallisation from Sr–Ti amorphous gel-like precursors occurs in the absence of crystalline surfaces and often produces mesocrystals by oriented aggregation of the primary nanocrystals. These considerations have a general validity and can be extended to many ternary and even more complex oxides.

Received 3rd May 2017,
Accepted 7th June 2017

DOI: 10.1039/c7ce00834a

rsc.li/crystengcomm

Institute of Condensed Matter Chemistry and Technologies for Energy, National Research Council, Via De Marini 6, I-16149 Genoa, Italy.
E-mail: vincenzo.buscaglia@ge.icmate.cnr.it

Giovanna Canu

Giovanna Canu is currently a researcher at the Institute for Condensed Matter and Technologies for Energy of the National Research Council of Italy. She has worked in the field of materials science, carrying out her activity in different laboratories. In particular, she has experience in oxide powder synthesis, oxide film deposition and ceramics. She is familiar with the most common morphological and structural characterisation methods for powders, ceramics and films, and with the dielectric and electrical characterisation of films and ceramics.

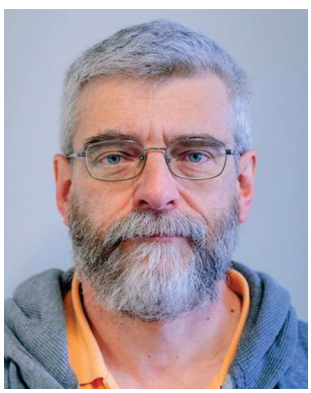

Vincenzo Buscaglia

Vincenzo Buscaglia, born in 1958, won a position at the National Research Council of Italy in 1985. He is currently a senior researcher at the Institute of Condensed Matter Chemistry and Technologies for Energy. His main research interests include the synthesis of functional oxides with a perovskite structure and the composition–microstructure–property correlations in dielectric and ferroelectric ceramics. He authored/co-authored about 145 papers in international journals.

1. Introduction

Strontium titanate, $SrTiO_3$, has recently attracted large interest as a multifunctional oxide with many different physical properties, such as electronic and ionic conductivity, thermoelectricity, strain-induced ferroelectricity, flexoelectricity, dielectric tunability and other field-dependent properties, which make it promising for several applications in the form of single crystal, ceramics, thin film and powder. The properties can be easily modified and adapted to the specific application by changing the nature and concentration of lattice defects through doping and controlling the oxygen stoichiometry.[1] In the case of epitaxial thin films, the properties can be altered by changing the nature of the substrate and, consequently, by varying the growth direction and the strain.[2] $SrTiO_3$ has widely been investigated for its photocatalytic properties and, in particular, as a photocatalyst for water splitting under light irradiation ("artificial photosynthesis") and photodegradation of organic and inorganic pollutants.[3] In contrast to TiO_2, $SrTiO_3$ photoelectrodes can split water without an external electric bias[4] because of the more suitable band structure of titanate. Moreover, Rh-doped $SrTiO_3$ is one of the rare oxide photocatalysts that can efficiently produce H_2 under visible light irradiation.

Between 110 and 2353 K (the melting point), strontium titanate exhibits the ideal cubic perovskite structure (space group $Pm\bar{3}m$). In the unit cell, the Sr^{2+} ions (ionic radius: 1.44 Å) are located on the corner of the cube whereas the smaller Ti^{4+} ion (ionic radius: 0.605 Å) is at the centre of the cube and is 6-fold coordinated by oxygen ions located at the centre of the faces of the cube. When cooled below ≈110 K, it undergoes a second order improper ferroelastic phase transition to a tetragonal structure ($I4/mcm$) associated with antiphase rotations of the oxygen octahedra around one of the <100> axes.[5] Thanks to its simple crystal structure, the effective property control by doping and the easy processing of single crystals, particles and ceramics, $SrTiO_3$ can be considered as a model perovskite for fundamental and applied science studies. A further advantage of strontium titanate is its high thermodynamic stability; it does not decompose under reducing conditions even at high temperature, differently from many other oxide perovskites, and shows good chemical and redox stability.[1,6]

The conventional preparation of strontium titanate is by solid-state reaction between $SrCO_3$ and TiO_2. However, the powders obtained with this method usually have low specific surface area (SSA) and consist of relatively coarse particles (≈1 μm) not suitable for neither photocatalytic applications nor the processing of dense ceramics with submicron or nanosized grains. Among alternative preparation methods (sol–gel, modified Pechini, peroxy-based route, molten salt, template-assisted chemical methods, mechanochemical, combustion, *etc.*[7–17]), hydrothermal synthesis has two main advantages: (i) it enables the preparation of very pure and extremely fine powders with high specific surface area (SSA up to ≈100 $m^2\ g^{-1}$) in a single step without the need of an additional annealing treatment to induce or improve crystallinity and, even more importantly, (ii) the particle size and morphology can be easily controlled and designed by changing the temperature, reaction time, precursor nature, and precursor concentration and by adding growth modifiers such as polar organic molecules and hydrophilic polymers. From this point of view, hydrothermal synthesis offers unique opportunities in comparison with other methods. The process can produce structures with different morphologies such as equiaxed particles, platelets, rods, wires, mesocrystals, superstructures and heterostructures with sizes ranging from 10 nm to several microns and properties suitable for many modern applications.[18] In particular, the size, shape and crystallinity of the particles, as well as the kind of exposed crystallographic surfaces and the existence of nanosteps on the crystal surface, have a strong impact on the photocatalytic properties.[3] Hydrothermal synthesis is one of the preferred methods to prepare pure and doped nanocrystalline $SrTiO_3$ photocatalysts (see, for example, ref. 19 and 20).

The aim of this paper is threefold: (i) to summarise the recent developments on the hydrothermal synthesis of pure and doped $SrTiO_3$, (ii) show the potential of this method for designing functional and catalytic materials with superior properties and (iii) present and analyse the hydrothermal crystallisation mechanisms. The main conclusions, including thermodynamic and kinetic aspects, have a general validity which goes beyond the specific compound and can be extended to many ternary and more complex oxides.

A concise overview of the physical and catalytic properties of $SrTiO_3$ is given in section 2. Section 3 is devoted to the hydrothermal synthesis, starting from the thermodynamic description and modelling of the hydrothermal reactions and then describing in detail the various strategies for morphology control and design. The hydrothermal crystallisation mechanisms are discussed in section 4. Specific defects associated with the hydrothermal synthesis are briefly reviewed in section 5. The present paper has not the ambition to be a complete review, but the examples have been chosen to illustrate some key aspects in the hydrothermal synthesis of strontium titanate and provide the reader with some general guidelines to design materials oriented to specific applications.

2. Physical and photocatalytic properties of $SrTiO_3$

2.1 Physical properties

The main physical properties and applications of strontium titanate[21–54] are summarised in Table 1. Pure $SrTiO_3$ is a semiconductor with an indirect band gap of 3.25 eV and a direct band gap of 3.75 eV (ref. 55) and also a quantum paraelectric (or incipient ferroelectric) material. Its low temperature dielectric constant increases up to very high values (≈10^4) with decreasing temperature and then remains constant below 4 K.[21] The transition to the ferroelectric phase is hindered by quantum fluctuations. Ferroelectricity can be

Table 1 Physical properties and applications of $SrTiO_3$ and $SrTiO_3$-based materials

Property	Notes	Application	Ref.
Ferroelectricity	Induced by doping, isotopic substitution, stress and strain	Non-volatile memories, piezoelectric devices	2, 21–26
Flexoelectricity	Induced by a strain gradient		27
Dielectric tunability	High tunability (up to 10 at 35 kV cm^{-1}) in $(Sr,Ba)TiO_3$	Varactors, MW filters	28–33
Large apparent dielectric constant	Electrically heterogeneous ceramics with semiconducting grains separated by an insulating grain boundary layer	Internal boundary layer capacitors (IBLC)	34, 35
High electronic conductivity and mobility	Induced by oxygen deficiency or donor doping. Conductivity (300 K) $\approx 10^3$ S cm^{-1} Hall mobility (300 K) ≈ 10 cm^2 V^{-1} s^{-1}	Anodes for SOFCs	1, 36–42
Mixed conductivity	Oxide ion and hole conductors	Cathode materials, MIEC membranes	43–45
Thermoelectricity	ZT up to 0.37	Thermoelectric generators (TGs)	37, 38, 46–48
Giant Seebeck effect	Thin film heterostructures	Miniaturised TGs	49, 50
Field-induced resistivity change and switching	Thin films	Memories, field-effect devices, MEMS	51–54

induced by doping (for example, substitution of Ca^{2+} (ref. 22) and Bi^{3+} at the Sr site[23]), oxygen isotope exchange[24] and stress or strain application.[2,25] Magnetoelectric coupling has been reported after doping with Mn^{2+} at the Sr site.[26] Application of a strain gradient to a $SrTiO_3$ single crystal produces a polarisation through the flexoelectric effect.[27]

The undoped stoichiometric material is a good insulator with a room-temperature dielectric constant of 300 and a low loss tangent (10^{-2}–10^{-3}) even at microwave frequencies.[28] One of the most interesting properties of ferroelectric materials for microwave applications is the strong dependence of their dielectric constant on the applied electric field, which makes ferroelectrics attractive for the fabrication of variable capacitance devices (varactors), microwave filters and phase shifters. This dependence is expressed by the tunability, *i.e.* the ratio between the dielectric constant measured in the absence of an applied field and the dielectric constant measured at a given field. $SrTiO_3$ has good tunability only at low temperature,[28–30] but $(Ba,Sr)TiO_3$ solid solutions and related composites show very high tunability (up to 10 at 35 kV cm^{-1}) even at room temperature.[28,31–33] Strontium titanate ceramics doped with small amounts of different oxides show very high values of the apparent dielectric constant (up to 2×10^4) and can be used for the manufacturing of internal barrier layer capacitors (IBLCs).[34,35] The electrically heterogeneous structure of these ceramics, composed of semiconducting grains with low resistivity and a highly insulating grain boundary layer, is responsible for the peculiar dielectric properties.

High electronic conductivity with metallic behaviour can be induced in strontium titanate by donor doping (incorporation of La^{3+} on the Sr site or Nb^{5+} on the Ti site) or processing in a reducing atmosphere leading to oxygen deficiency.[36–38] Conductivity values up to 10^3 Scm^{-1} and an electron mobility of 10 cm^2 V^{-1} s^{-1} have been reported at room temperature. The carrier mobility increases rapidly with decreasing temperature and can achieve values exceeding 3×10^4 cm^2 V^{-1} s^{-1} at low temperature.[39] Because of its high conductivity together with its stability in reducing atmospheres, donor-doped $SrTiO_3$ has widely been investigated as an anode material for solid-oxide fuel cells (SOFCs).[1,6,40–42] When doped with acceptors, strontium titanate exhibits mixed ionic (oxygen) and hole conductivity[43–45] with potential application as a cathode material in SOFCs. As a model perovskite, the high-temperature defect chemistry of pure and doped $SrTiO_3$ has been investigated in detail[43,56] and the enthalpies corresponding to the most common defect reactions are available.

Donor-doped strontium titanate also shows a negative and relatively large Seebeck coefficient ($S = -200$ to -400 μV K^{-1} at room temperature) and is a potential n-type thermoelectric material for high temperature applications.[37,38,46–48] However, the high thermal conductivity ($\approx$10 W m^{-1} K^{-1} at room temperature) limits the maximum attainable value of the thermoelectric figure-of-merit ZT ($\approx$0.37 at 1000 K). Enhancement of the Seebeck coefficient up to $\approx -10^3$ μV K^{-1} was reported in thin film heterostructures consisting of alternating $SrTiO_3$ and TiO_2 layers.[49] More recently, high negative S values of the order of -10^4–-10^5 μV K^{-1}, oscillating at regular intervals as a function of the gate voltage, have been reported for $LaAlO_3/SrTiO_3$ heterostructures at 4.2 K.[50] In both cases, the enhancement has been correlated with the existence of a 2D electron gas at the interface.[57] The electrical conductivity of thin-film $SrTiO_3$ structures can be controlled by the application of an external electric field and this effect can be exploited for the fabrication of electronic components such as memory and field-effect devices.[51–54] Last but not least, single-crystal strontium titanate is one of the most common substrates used for the growth of epitaxial thin films of many different perovskites.

2.2 Photocatalytic properties

Only a very short overview on the photocatalytic properties of $SrTiO_3$-based materials will be given here. A more exhaustive presentation of this broad and complex topic can be found in ref. 3 and references therein. Binary and ternary oxides such

as TiO_2, $KTaO_3$ and $SrTiO_3$ possess suitable band structures for water splitting. In particular, TiO_2 has been extensively investigated for a long time. Water splitting by UV light was first demonstrated by Fujishima and Honda using a TiO_2 photoelectrode and applying an external bias.[58] However, powdered TiO_2 cannot split water unless a co-catalyst is used because the conduction band level is not high enough to efficiently reduce water to H_2. In contrast, $SrTiO_3$ and $KTaO_3$ photoelectrodes with a perovskite structure can split water without an external bias because of their higher conduction band levels and can be used as powder photocatalysts.[3] The attention has mainly focused on the study of nanopowders and nanocrystalline materials because of their high specific surface area. The presence of a co-catalyst such as Pt, RuO_2 and NiO can enhance the activity of the photocatalyst by increasing the number of sites for hydrogen reduction and evolution. A co-catalyst for water oxidation is usually unnecessary. The co-catalysts should not accelerate the back reaction corresponding to the recombination of oxygen and hydrogen in water, as it happens with Pt. For example, NiO-loaded $SrTiO_3$ can split liquid and vapour water in H_2 and O_2 without recombination.[59] More recent studies have shown that NiO–$SrTiO_3$ is more likely a three-component Ni–NiO–$SrTiO_3$ system in which $SrTiO_3$ absorbs light, Ni reduces protons, and NiO oxidises water.[60] Owing to their band gap (3.4–3.0 eV), the above-mentioned photocatalysts are not suitable to work with visible light, as the band gap should be <3.0 eV ($\lambda > 415$ nm). Doping of TiO_2 and $SrTiO_3$ with Rh ions[61] or transition metal ion couples (Cr^{3+}/Ta^{5+}, Cr^{3+}/Sb^{5+}, Ni^{2+}/Ta^{5+})[62–64] is effective in sensitisation of $SrTiO_3$ to visible light; these ions form additional levels within the band gap thus resulting in visible light response. Doping with acceptor/donor couples at the Ti site does not require the formation of charge compensating defects, such as cation and oxygen vacancies, which act as recombination centres for the electron/hole couples, thus avoiding an activity reduction. Rh:$SrTiO_3$ is one of the rare oxides that can split water under visible light with high efficiency without the need of a second dopant.[61]

Strontium titanate has also been investigated as a photocatalyst for the degradation of organic and inorganic compounds[7,15,17,65,66] and CO_2 reduction.[67] Heterojunctions of $SrTiO_3$ with other semiconductors[68–72] have shown enhanced catalytic activity in comparison with the isolated components. The coupling of two semiconductors in suitable nanoarchitectures can facilitate the separation of the photogenerated electron–hole couples and provide a higher number of active sites for the redox reactions. In the case of Cr:$SrTiO_3$/TiO_2 heterojunctions[68] under visible light illumination, the photogenerated electrons of Cr-doped $SrTiO_3$ are photoexcited from the valence band (Cr 3d) to the conduction band (Ti 3d) and then transferred to the conduction band of TiO_2 because the conduction band of $SrTiO_3$ is 200 mV more negative than that of TiO_2. $SrTiO_3$ has also been investigated as a photoelectrode material for photosensitised solar devices, although less efficient than TiO_2 anatase.[73]

3. Hydrothermal synthesis

3.1 Generalities

The hydrothermal method has become one of the most popular techniques for the advanced synthesis of a large number of compounds, including simple and complex oxides, chalcogenides, carbonates, silicates, silicoaluminates, *etc.*[18,74–78] The term "hydrothermal synthesis" usually refers to the crystallisation of substances by means of heterogeneous reactions in aqueous media above 100 °C and 1 bar. The method exploits the strong acceleration of heterogeneous reactions and the increased solubility of most inorganic compounds in hot water. Solvothermal synthesis can be considered as a generalisation of the hydrothermal method when water is replaced by organic or mixed water–organic solvents. However, when high boiling point organic liquids are used, the application of pressure is not always required. Also, the growth of crystals in supercritical fluids represents an extension of the hydrothermal process. The same solution chemistry and crystallisation mechanism often dominate over a wide range of experimental conditions and, consequently, the terms "hydrothermal" and "solvothermal" should not be taken too narrowly.

Solvent-mediated crystallisation under hydrothermal conditions has a fundamental role in the cold sintering process of ceramics and ceramic–polymer composites.[79,80] With this recent and revolutionary technology, high densification can be attained at temperatures lower than 200 °C utilising a transient solvent, water or a water solution of inorganic salts, which control the dissolution and re-precipitation of the inorganic compound.

Hydrothermal synthesis is industrially used for the production of different materials. Large synthetic quartz crystals, gems and other single crystals of commercial value, including $Be_3Al_2(SiO_3)_6$ (beryl, emerald, aquamarine), Al_2O_3 (corundum, ruby, sapphire), $BeAl_2O_4$ (chrysoberyl, alexandrite) and ZnO (zincite) are grown with this method. High quality hydrothermal α-Al_2O_3 powders are used as abrasives and for the plasma spray technology. Large amounts of fine perovskite powders, including $BaTiO_3$, $Ba(Ti,Zr)O_3$ and $(Ba,Sr)TiO_3$, are produced *via* a hydrothermal route by Japanese companies for the multilayer ceramic capacitor industry. Synthetic zeolite catalysts for the petrochemical industry are also of hydrothermal origin.

At the laboratory scale, the hydrothermal/solvothermal method has proven to be extremely useful to synthesise new compounds, to grow crystals of metastable phases or compounds which cannot be obtained by other methods, and, in recent years, for the synthesis of a huge variety of nanoparticles and nanostructures with different morphologies, including nanowires, nanotubes, hollow particles, mesocrystals and thin films.[18,76–78] Hydrothermal reactions are commonly carried out under isothermal conditions in small steel autoclaves (internal volume 50–500 mL) with Teflon or glass lining to prevent corrosion of the internal cavity. The simplest and cheapest equipment is represented by an acid digestion

bomb, which can operate at temperatures up to 250 °C. This kind of reactor is not stirred and, consequently, crystallisation occurs under stagnant conditions and will be dominated by diffusive mass transport. Furthermore, the sedimentation of the solid phase at the bottom of the vessel can have a strong impact on reaction kinetics and product morphology. Nevertheless, acid digestion bombs are largely used for lab-scale hydrothermal synthesis.

Hydrothermal $SrTiO_3$ is usually prepared by reacting a TiO_2 powder (rutile or anatase or amorphous titania) with a soluble Sr salt ($SrCl_2$, $Sr(NO_3)_2$, $Sr(OH)_2$) in a highly alkaline environment. The same approach applies to many other ABO_3 compounds where A = Ca, Sr, Ba, Pb and B = Ti, Zr, Hf. A notable exception occurs for tin, as the hydrothermal synthesis produces the hydroxostannate $ASn(OH)_6$ rather than the ternary oxide. When the Ti precursor is a solution of a soluble Ti compound such as $TiOCl_2$, a Ti alkoxide or titanium bis(ammonium lactato)dihydroxide (TALH), rapid hydrolysis occurs at the alkaline pH needed for the reaction with formation of an amorphous hydrous titania gel-like precipitate (AHT), sometimes indicated as "Ti hydroxide" or "$Ti(OH)_4$", which is in fact the effective precursor. Very reactive gel-like precursors can be obtained by hydrolysing a mixed Sr–Ti solution by addition of a strong base – either NaOH or KOH.

3.2 Thermodynamic considerations

Hydrothermal reactions involve the interaction between neutral and ionic species in aqueous solution and one or more solid phases. The equilibrium concentration of aqueous species and the amount of solid phases can be obtained by solving a system of linear and non-linear equations including chemical equilibrium reactions, mass balance equations and the electroneutrality constraint, provided that reference thermodynamic data are available for all species.[81] Thus, the evolution of the equilibrium composition as a function of fundamental physico-chemical variables such as temperature, pressure, pH and reactant concentration can be predicted. The results are usually presented as stability diagrams in which the stable solid phases and the predominant aqueous species are reported as a function of pH and the concentration of one of the reactants. Thermodynamic modelling of the hydrothermal synthesis of perovskites and in particular alkaline-earth and lead titanates was developed by Riman and co-workers.[81–83] As shown in the A–Ti–H_2O stability diagram (Fig. 1), the formation of $ATiO_3$ (A = Ca, Sr, Ba) by reaction of TiO_2 with a solution of an alkaline-earth salt requires an alkaline pH (7.2 for $SrTiO_3$ and 8.3 for $BaTiO_3$ when the molality (m_M) of the solution is 10^{-2}). The minimum required pH increases with decreasing A concentration. Quantitative precipitation (yield >99.995%) requires higher pH values (9.6 for $SrTiO_3$ and 10.8 for $BaTiO_3$ for $m_M = 10^{-2}$). Thus the addition of a highly dissociated hydroxide ("mineraliser"), such as NaOH or KOH, is required unless $Sr(OH)_2$ and $Ba(OH)_2$, which are rather strong bases, are used as precursors. At neutral or acidic pH, $BaTiO_3$ and $SrTiO_3$ are unstable and release alkaline-earth cations. Barium titanate is less stable than $SrTiO_3$ and $CaTiO_3$. More recent calculations[84] have confirmed that $SrTiO_3$ is the predominant solid phase over the whole range of explored conditions: T = 25–300 °C, m_{NaOH} = 0.01–2 mol kg^{-1}, m_{Sr} = 0.05–0.2 mol kg^{-1}. However, as already pointed out by Lencka and Riman,[81,82] the presence of carbon dioxide or carbonate ions in the reaction vessel can often result in the formation of an alkaline-earth carbonate as a side-product, owing to the high stability of these compounds.

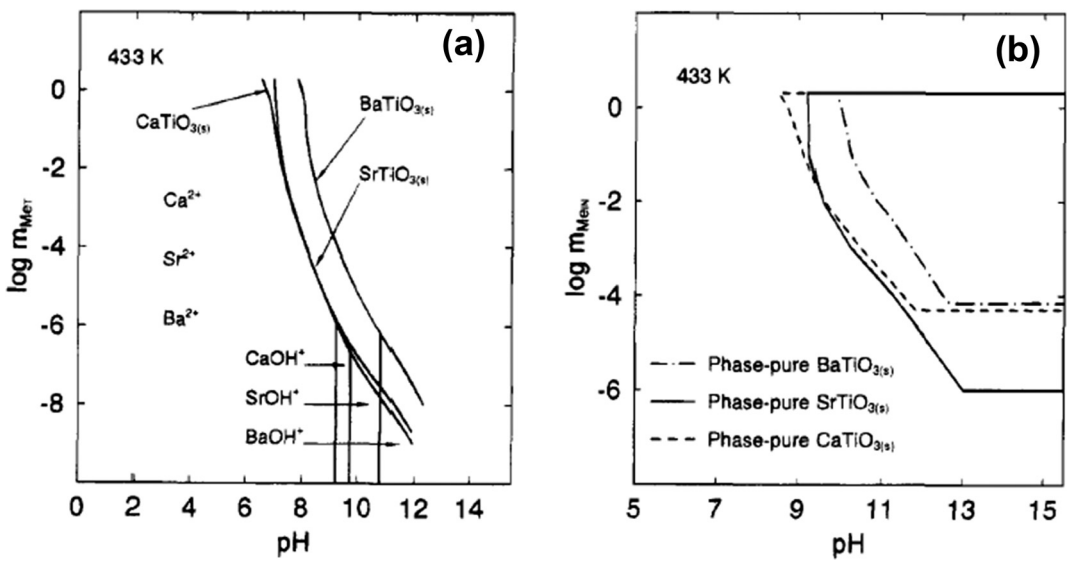

Fig. 1 (a) Calculated phase stability diagrams of A–Ti–H_2O systems (A = Ca, Sr, Ba) at 160 °C and A/Ti molar ratio = 1. The continuous lines indicate the onset of perovskite formation. The leftmost curve refers to $CaTiO_3$ formation. (b) Regions corresponding to quantitative (yield >99.995%) formation of $ATiO_3$ (A = Ca, Sr, Ba). The vertical axis reports the molality of the alkaline-earth cation. Reprinted with permission from ref. 82. Copyright 1995 American Chemical Society.

Assuming a maximum amount of $SrCO_3$ corresponding to 2 mol% of the overall strontium concentration, the calculations have confirmed that formation of strontium carbonate always occurs under the above reported conditions.[84] The carbonate usually disappears after calcination as it reacts with the residual titania precursor, provided that Sr and Ti were in stoichiometric ratio. The formation of $SrCO_3$ can be largely suppressed by using strontium salts and NaOH/KOH from sealed bottles and avoiding the contact of the precursor solution with air.

The pH also has a strong kinetic effect on the hydrothermal reaction. Titania is an amphoteric oxide and its solubility rises at both low and high pH values,[85] as shown in Fig. 2 for rutile. At intermediate pH values (3–9), the solubility of rutile is independent of pH and only slightly dependent on temperature. In this region, the predominant aqueous titanium species is $Ti(OH)_4$. Below a pH of 3, the solubility rises with decreasing pH owing to the formation of $Ti(OH)_3^+$. The formation of $Ti(OH)_5^-$ and $Ti(OH)_6^{2-}$ at pH > 10 is responsible for the rapid solubility increase observed in alkaline solutions. The increase of solubility determines the increase of the driving force (supersaturation) and, consequently, of the crystallisation rate of the reaction product.

The TiO_2 solubility at high pH is greatly dependent on temperature. In a 1 m NaOH solution, the rutile solubility increases from 1×10^{-5} m at 100 °C to 1×10^{-4} m at 300 °C.[85] It is worth noting that, for a given base concentration, the pH strongly decreases with increasing temperature. In the case of the 1 m NaOH solution, the pH drops from 13.8 at room temperature to 10.4 at 325 °C.[85] This observation is also confirmed by the thermodynamic calculations and is a consequence of the temperature dependence of the ionic product of water. The decrease of pH with increasing temperature and the need to increase the solubility of precursors explains, at least partially, the common practice of using a strong excess of mineraliser to promote the formation of the final product.

Furthermore, the solubility of titania depends on the specific polymorph considered (rutile, anatase, amorphous hydrous titania – "$Ti(OH)_4$"),[84] as is evident from Fig. 3. The curves correspond to a solution containing 0.2 mol L^{-1} $Sr(OH)_2$ and 0.833 mol L^{-1} NaOH. The solubility was calculated by considering the starting titanium compound in the reaction environment and equilibrating the system while inhibiting the formation of any other solid phase. The aqueous species $Ti(OH)_n^{(n-4)-}$ (n = 4–6) predominate at pH ≥ 7 and $Ti(OH)_6^{2-}$ is the major one under strong alkaline conditions. The solubility of rutile is rather low and ranges between 2×10^{-6} m at 20 °C and 2×10^{-4} m at 320 °C. The calculated values are in good agreement with the experimental data in 1 m NaOH reported by Knauss *et al.*[85] in the whole temperature range. The solubility of anatase is 3–10 times higher than that of rutile and at room temperature is comparable (as order of magnitude) with the data extrapolated from Schmidt and Vogelsberger's experimental results.[86]

The solubility of "$Ti(OH)_4$" is more than 2 orders of magnitude higher than that of rutile and attains 2.5×10^{-3} m at 200 °C. The room temperature solubility of freshly prepared amorphous $Ti(OH)_4$ was reported to be 3×10^{-6} M at pH values in the range 5–12,[87] *i.e.* about 300 times higher than that of rutile at 100 °C and pH 3–10.[85] A moderate solubility of ≈0.01 M at RT was determined by Kostrikin *et al.*[88] in 1 M NaOH. The supersaturation follows the same order of solubility: rutile < anatase < "$Ti(OH)_4$". Thus crystallisation of $SrTiO_3$ from "$Ti(OH)_4$" or, more generally, AHT precursors is predicted to occur in a shorter time or at lower temperature in comparison with anatase and rutile. Accordingly, formation of the perovskite from the hydrolysis products of $TiOCl_2$

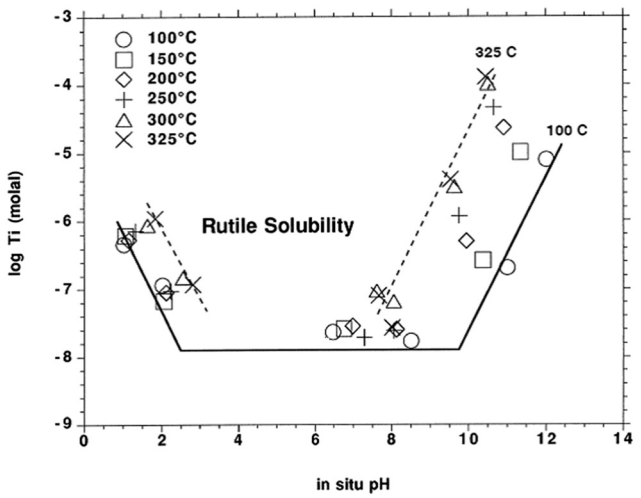

Fig. 2 Solubility of rutile TiO_2 as a function of pH at different temperatures from 100 to 325 °C. The lines are a guide for the eye for the following temperatures: 100 °C (continuous line) and 325 °C (dashed line). Adapted from from ref. 85, copyright 2001, with permission from Elsevier.

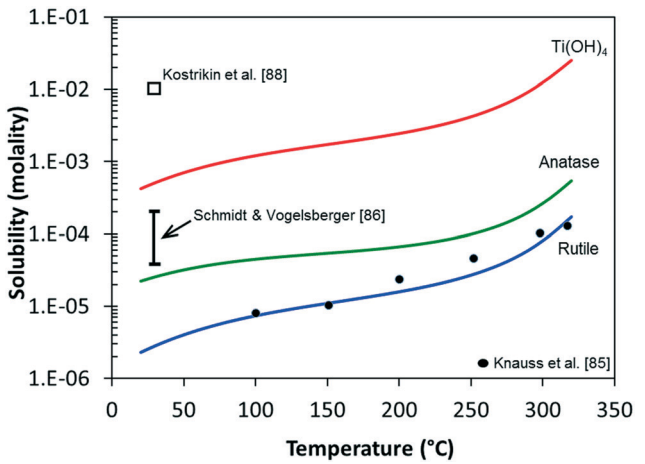

Fig. 3 Calculated solubility of rutile (blue line), anatase (green line), and $Ti(OH)_4$ (red line) in a mixed $Sr(OH)_2$ (0.2 M)–NaOH (0.833 M) water solution (see text for details). Experimental solubility data of TiO_2 polymorphs measured in 1 M NaOH solution are reported for comparison. Adapted with permission from ref. 84. Copyright 2015 American Chemical Society.

and Ti alkoxide solutions is commonly observed at 70–90 °C (ref. 89–93) and sometimes at even lower temperatures. For example, quantitative crystallisation of $SrTiO_3$ in less than 2 hours occurred at 45 °C when the synthesis was carried out from an amorphous gelatinous suspension obtained by rapid hydrolysis of a mixed $SrCl_2$–$TiOCl_2$ solution.[94] As with many other gels, this precursor has a polymeric network structure with pores and channels with sizes from a few nanometres to a few tens of nanometres filled by the solvent.[92,95,96] Alkaline-earth ions do not take part in the formation of the network and remain in solution or are adsorbed on the gel surface. In addition to the higher solubility, the huge contact area of the gel network with the solvent will further promote a faster reaction in comparison with anatase and rutile.

3.3 Morphology control

The size and morphology of particles produced by hydrothermal/solvothermal synthesis can be easily and actively controlled by varying several experimental parameters, including the precursor nature and concentration, temperature, reaction time and solvent composition, as also discussed by Huang *et al.*[97] This is the main advantage of this synthetic route in comparison with other methods such as sol–gel synthesis, modified Pechini method, molten salt synthesis and combustion methods.[7–17] In the next paragraphs, representative examples of several kinds of morphologies will be presented and discussed.

3.3.1 Fine equi-axed particles. The $SrTiO_3$ surfaces with the lowest energy are the {100} surfaces[98] and, consequently, solvent-mediated crystallisation of the perovskite in the absence of growth modifiers and other additives produces cubic particles. The edges and corners of the crystals are often truncated by 110 and 111 surfaces, respectively.[98,99] Depending on the precursor concentration, temperature and reaction time, the size of the particles can be tailored from the nanometre to the micron scale length. As an example, cubic particles with edge lengths in the range 80–1400 nm were produced by heating Sr–Ti gel suspensions with Sr concentrations in the range 0.025 to 0.09 M and a Sr/Ti molar ratio of 1.1 at 55–95 °C.[94]

Specific additives which adsorb at the solid surface are widely used to produce small nanoparticles with narrow size distribution by suppressing particle growth and disordered aggregation. The same additives can be used to tailor, at least to some extent, the particle shape. Oleic acid (OLA) is a quite effective molecule and the particle size can be reduced in the range 10–20 nm[100–103] by OLA addition. Its polar carboxylic group adsorbs on the oxide surface while the alkyl tail remains oriented outwards. The size of the perovskite nanocrystals hydrothermally synthesised at 200 °C using TALH as a precursor could be varied between 10 and 100 nm by adding oleic acid and hydrazine in different molar ratios.[100] Spontaneous self-assembly of the OLA-capped $SrTiO_3$ nanocrystals with formation of 2D arrays occurred when the suspension was poured on a substrate and the solvent evaporated, owing to the attractive interactions between the alkyl chains located on different particles. $SrTiO_3$ nanocubes with edges of 15–20 nm were obtained by hydrothermal treatment of microemulsions prepared using OLA as surfactant.[103] Formation of $SrTiO_3$ nanorods and their rapid ordered aggregation was also ascribed to the addition of OLA.[104] Very stable sols containing nearly monodisperse $SrTiO_3$ nanocubes with a size of 8 nm were obtained by solvothermal reaction at 160 °C in triethylene glycol, adding polyvinylpyrrolidone (PVP) as a capping agent.[105] The synthesis of very small (5 nm) and non-aggregated particles of $SrTiO_3$ without the need of capping molecules was performed by dissolving metallic strontium in benzyl alcohol, adding Ti-isopropoxide and heating at 200 °C, as described by Niederberger *et al.*[106]

The solvent composition also has a significant effect on both particle size and shape. According to Dong *et al.*,[107] when water–alcohol mixtures were used as solvent, the crystal habitus could be altered by increasing the pK_a of the alcohol and evolved from perfectly cubic (ethanol, 1,4-butanediol) to predominantly rhombododecahedral (ethylene glycol, pentaerythritol), as shown in Fig. 4. Hydrothermal reaction at 140 °C of a titanium–triethanolamine complex with $Sr(OH)_2$ in mixed polyol–water mixtures produced cubic or spherical particles whose diameter was controlled by the polyol/water volume ratio.[108] In particular, when the polyol was ethylene glycol (EG), the diameter of the particles could be controlled between ≈20 and ≈100 nm by decreasing the water/EG ratio. Formation of nanoflakes that originated from ordered aggregation of primary nanocrystals of ≈10 nm was observed with EG-rich mixtures. The diameter of $SrTiO_3$ spherical particles obtained at 200 °C from amorphous titania and Sr nitrate was determined by the number of alkyl groups bonded to the nitrogen atom in the amine used as solvent.[109] Monoethanolamine and triethanolamine produced particles of 100–150 and 50–70 nm, respectively.

3.3.2 Porous particles. The synthesis of porous and especially mesoporous submicrometric $SrTiO_3$ particles has received attention as an approach to increase the surface area and, consequently, the catalytic properties, avoiding the complications related to the manipulation and separation of extremely fine nanoparticles. In most cases, porous particles were prepared starting from spheres of AHT with a diameter of a few hundred nanometres obtained by controlled hydrolysis of Ti alkoxides.[110–113] These spheres are highly porous (SSA > 200 m^2 g^{-1}) and during the hydrothermal treatment are converted to the perovskite by reaction with the Sr^{2+} and OH^- ions diffusing inward through the channels existing in the amorphous structure. Consequently, the spherical morphology of the precursor is preserved. The method is quite general and can be extended to the synthesis of $BaTiO_3$, $PbTiO_3$ and $Pb(Zr,Ti)O_3$ porous spherical particles.[110] The pore size of $SrTiO_3$ can be controlled in the range 8.5–16.1 nm by changing the reaction time and the concentration of polyvinyl alcohol (0–8 g L^{-1}) added as a pore templating agent.[113] The SSA can exceed 100 m^2 g^{-1}. The final spheres look like porous single crystals or mesocrystals with

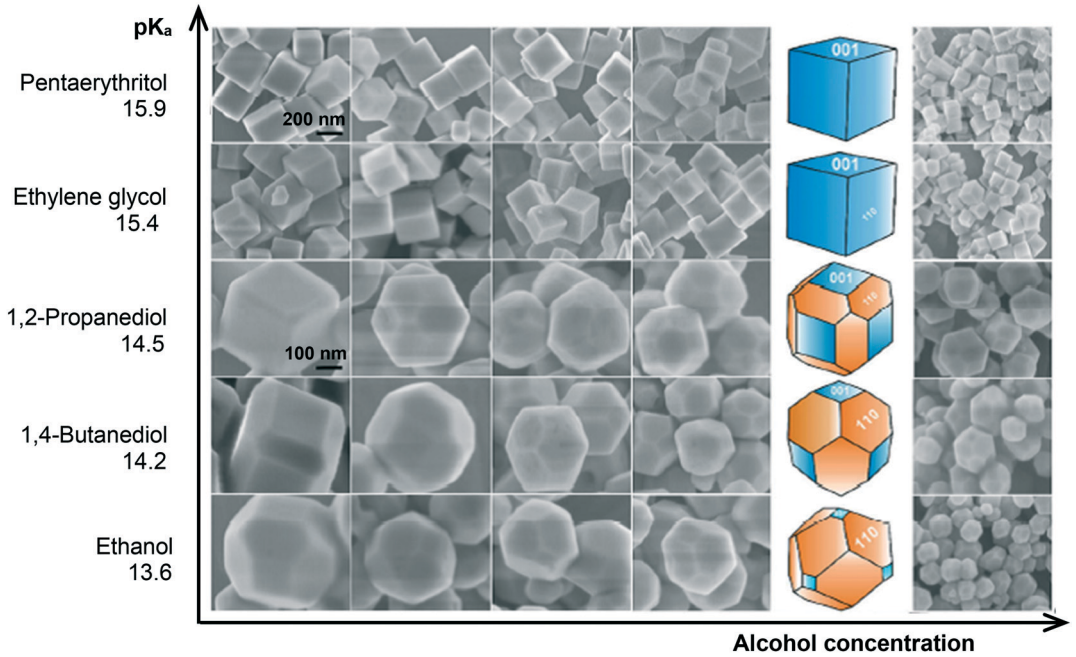

Fig. 4 SEM images of the $SrTiO_3$ particles synthesized in water–alcohol mixtures using alcohols with different pK_a values and varying alcohol concentration. Adapted from ref. 107 with permission of Springer. Copyright 2014 Springer. See the original paper for details.

crystalline regions of tens of nanometre in size separated by a mesopore network, as indicated by the electron diffraction pattern and the HRTEM observation.

Amorphous spherical particles of $ATiO_3$ (A = Ba, Sr, Ca) were obtained by reaction between amorphous titania and $A(OH)_2$ in ethanol at room temperature. Calcination at 800–900 °C resulted in the formation of monodisperse porous crystalline perovskite spheres with a diameter of 1–2 μm.[114] More recently, porous $SrTiO_3$ particles with enhanced photocatalytic activity for water splitting were prepared by hydrothermal reaction at 150–180 °C of flower-like spherical particles (0.6–0.8 μm) of hydrogen titanate $H_2Ti_2O_5{\cdot}H_2O$ in the presence of the surfactant cetyltrimethylammonium bromide (CTAB).[115] The final particles are produced by the *in situ* conversion of the templates and consist of ordered aggregates of primary nanocubes (60–80 nm) with the same crystallographic orientation separated by nanopores of 10–20 nm (Fig. 5a). The morphology of both the porous aggregates and the primary units is very sensitive to the reaction time and temperature and dominated by local-scale recrystallisation processes. Similar morphologies are also described in ref. 116. Porous aggregates and spherical particles of Cr-doped $SrTiO_3$ were prepared by hydrothermal treatment of a gel containing different metal ions. The SSA of the product ranged between 23 and 65 $m^2\ g^{-1}$ depending on the reaction temperature (80–200 °C).[117]

A second strategy for the preparation of mesoporous spherical particles is the addition, besides KOH and Sr nitrate, of sodium silicate to a suspension of freshly prepared AHT.[118,119] The hydrothermal reaction at 200 °C leads to the formation of small $SrTiO_3$ nanoparticles (5 nm) coated with a thin amorphous silica layer which spontaneously aggregate together in a partially ordered state. The diameter (150–300 nm), pore size (4.9–32.1 nm) and surface area (30–169 $m^2\ g^{-1}$) of the resulting mesoporous spheres can be tuned by varying the KOH concentration.

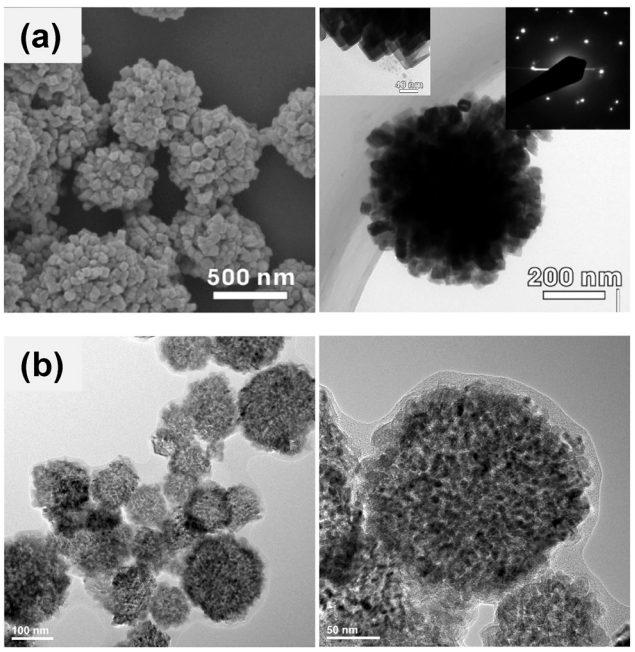

Fig. 5 Morphology of $SrTiO_3$ porous particles prepared by hydrothermal reaction of different precursors. (a) Flower-like $H_2Ti_2O_5{\cdot}H_2O$ particles reacted at 150 °C in the presence of cetyltrimethylammonium bromide. Reprinted with permission from ref. 115. Copyright 2013 American Chemical Society. (b) Gel-like suspension obtained by rapid hydrolysis of a $SrCl_2$-$TiOCl_2$ solution in the presence of oleic acid hydrothermally treated at 135 °C (unpublished results).

A further strategy is the removal of the organic component by thermal treatment of hybrid mesocrystals. Often the formation of mesocrystals through a process of oriented aggregation, as will be further discussed in section 4.3, is driven by organic molecules or polymers adsorbed at the surface of the primary nanocrystals. In this case, a consistent fraction of the organic molecules are trapped inside the mesocrystal together with small amounts of the solvent.[120] For example, $SrTiO_3$ spherical mesocrystals obtained by addition of citric acid or polyacrylic acid[94] exhibited a SSA of 130 m^2 g^{-1} after calcination at 400 °C. The formation of spherical porous mesocrystals is also promoted by the addition of OLA, as shown in Fig. 5b.

3.3.3 Particles with a highly anisotropic shape. The hydrothermal method is one of the most suitable approaches for the synthesis of particles with anisotropic shape, including nanorods, nanowires and nanoplatelets. Some examples are shown in Fig. 6. In particular, the preparation of $ATiO_3$ (A = Ca, Sr, Ba, Pb; B = Ti, Zr) nanowires and nanorods has been widely investigated[121] for potential application in energy harvesting microdevices, high energy density dielectric composites, and sensors. Two main synthetic strategies are used: (i) the direct growth from liquid phase (water, organic solvents, molten salt), often adding specific molecules as growth modifiers and (ii) the use of appropriate reactive templates. The direct growth produces single crystal wires with a well-defined morphology, but only a few reports exist in the case of strontium titanate. $BaTiO_3$ and $SrTiO_3$ nanowires with diameters of 50–100 nm and lengths of up to a few micrometres were grown at 170 °C by Joshi *et al.*[122] using an alkaline-earth hydroxide and titania particles as precursors and water as a solvent, adding ammonia as a mineraliser. Ammonia seems to be the key ingredient to inducing anisotropic growth. Solvothermal treatment at 280 °C for 6 h of bimetallic alkoxides, such as barium titanium isopropoxide and strontium titanium isopropoxide, dissolved in heptadecane with the addition of OLA resulted in the formation of perovskite thin nanowires (5–60 nm in diameter, Fig. 6a).[123]

A wider literature exists on templated growth.[124–131] The aim is to exploit a topochemical reaction between the template, usually a layered hydrogen or alkali titanate, and the A^{2+} ions in solution.[132] The crystallographic structure of these layered compounds corresponds to anatase-like layers consisting of corner-shared TiO_6 octahedra separated by interlayers containing alkaline or hydrogen ions and variable quantities of water.[133] Owing to the layered structure and weaker interactions along the stacking direction, the alkaline ions can be easily exchanged with ions of similar size, such as alkaline-earth cations. In a topochemical transformation, both the morphology and the crystallographic order of the template are preserved, thus enabling a high level of morphological control. Sometimes compounds with a wire-like morphology are generated as intermediate products during the hydrothermal treatment and act as effective reactive templates for the synthesis of $SrTiO_3$ and $BaTiO_3$ nanowires.[134–136] However, in several cases a topochemical transformation of the template in the $ATiO_3$ perovskite is not observed as the hydrothermal reaction is dominated by the heterogeneous nucleation of the perovskite on the surface of the template and

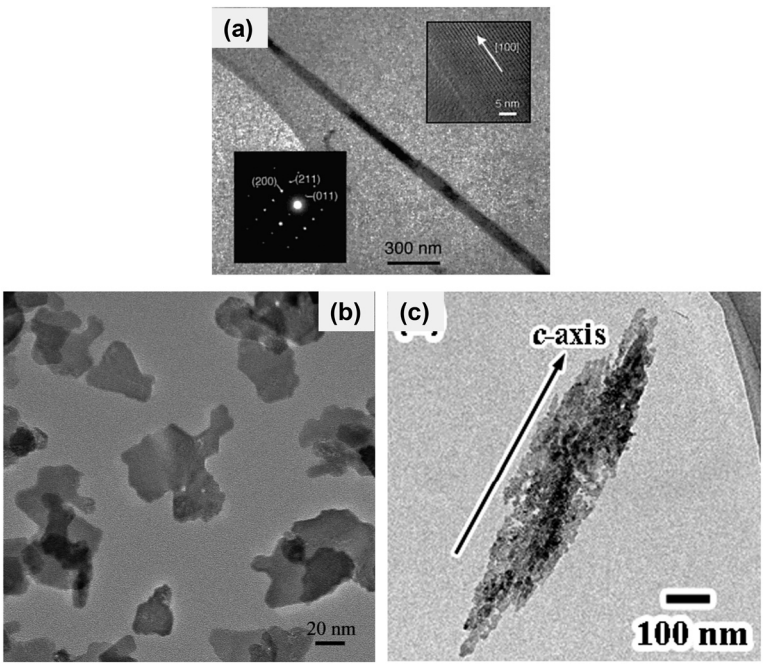

Fig. 6 (a) $SrTiO_3$ nanowires prepared by solvothermal synthesis in heptadecane in the presence of oleic acid. Reprinted with permission from ref. 123. Copyright 2002 American Chemical Society. (b and c) $SrTiO_3$ nanosheets prepared by solvothermal synthesis in either (b) ethylene glycol or (c) ethylene glycol/water mixed solvent. (b) Reprinted with permission from ref. 146. Copyright 2011 American Chemical Society; (c) reprinted from ref. 108, with permission from Elsevier.

dissolution–precipitation processes rather than ionic exchange. Consequently, the hydrothermal reaction often results in the formation of polycrystalline wires with a rough surface, dendritic crystals or even loose particles,[84,128–131] as also observed for $BaTiO_3$.[136–138] The final morphology is strongly dependent on the template composition, as recently shown for different single crystal templates (sodium titanate, hydrogen titanate, anatase and rutile) with the same wire morphology reacted under identical experimental conditions using $Sr(OH)_2$ as the strontium source and NaOH as the mineraliser.[84,131] The templates were obtained from sodium titanate nanowires by a series of topochemical manipulations to minimise the impact of precursor morphology and crystallographic order on the reaction. Despite a topochemical reaction being in principle possible, formation of perovskite particles with random orientation is observed on the surface of $H_2Ti_3O_7$ and $Na_2Ti_3O_7$ wires (Fig. 7a and b). The successive morphological evolution depends on the density of surface nuclei. In the case of $H_2Ti_3O_7$ wires, many of the perovskite crystals are isolated or poorly connected and, once the residual template which held together the $SrTiO_3$ particles is totally consumed, a powder composed of loose particles and irregular aggregates is obtained with almost complete loss of the initial wire morphology (inset of Fig. 7a). A similar evolution was reported in ref. 126–128. In contrast, polycrystalline wires with a rough surface are observed after complete reaction of the sodium titanate wires (Fig. 7b). In the case of anatase, the reaction involves the heteroepitaxial growth of $SrTiO_3$ leading to the formation of mesocrystals composed of arrays of crystallographically oriented nanocubes with a size of the order of

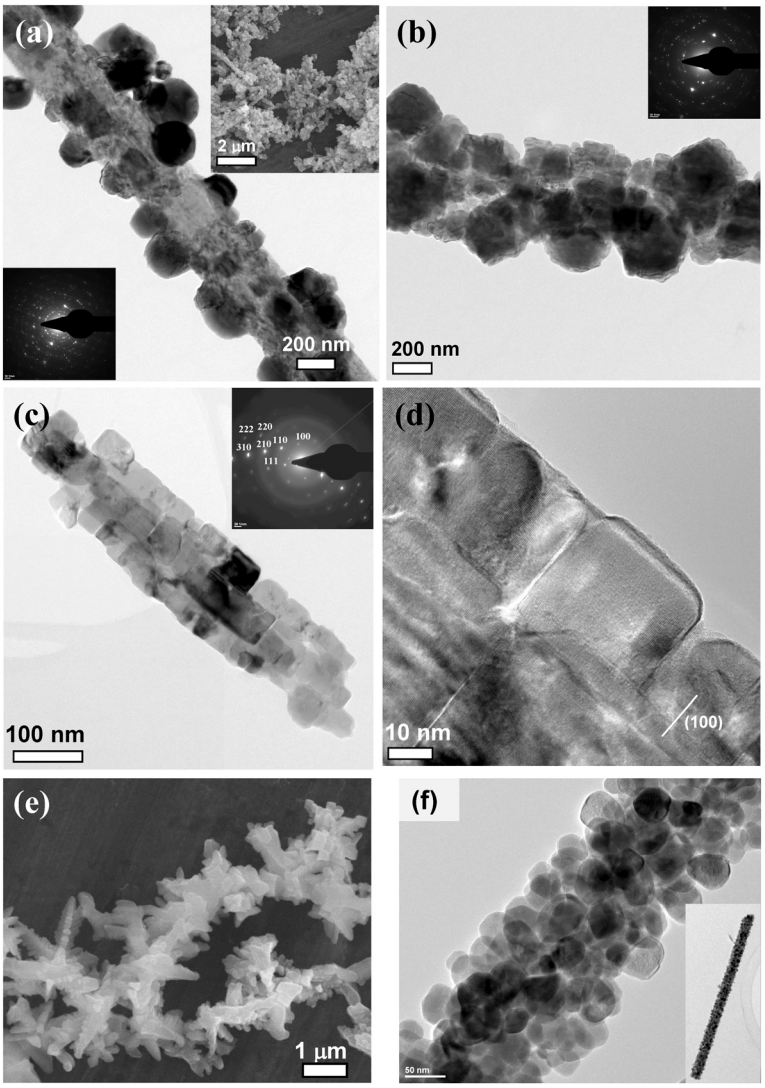

Fig. 7 Effect of different nanowire precursors on the morphology of $SrTiO_3$ obtained by hydrothermal treatment at 200 °C. (a) Precursor: $H_2Ti_3O_7$ wires, after 15 min. The inset in the right upper corner shows the loose particle morphology after 48 h. (b) Precursor: $Na_2Ti_3O_7$ wires, after 24 h. (c and d) Precursor: anatase, after 15 min. The insets in (a)–(c) show the ED patterns of the $SrTiO_3$ structures. (e) Precursor: rutile, after 48 h. (f) The same precursor and experimental conditions as in (a) but without a mineraliser (NaOH). The inset shows the overall morphology. (a, b and e) reprinted with permission from ref. 84; (c and d) reprinted with permission from ref. 131. Copyright respectively 2015 and 2012 American Chemical Society. (f) unpublished results.

50 nm (Fig. 7c and d). The initial wire-like morphology is largely maintained. Differently, growth of dendritic crystals is observed on the surface of rutile templates and the initial morphology is rapidly lost (Fig. 7e).

For a given template, the final morphology can be altered by changing the experimental conditions. For example, if the mineraliser (NaOH) is removed while keeping the other experimental parameters unchanged, according to ref. 84, the hydrothermal treatment of hydrogen titanate nanowires in a $Sr(OH)_2$ solution produces, after 24 h, polycrystalline wires with a cob-like morphology (Fig. 7f) rather than the loose particles shown in the inset of Fig. 7a. It is clear that the degree of crystallographic matching between the perovskite and the template as well as the supersaturation and the prevailing mass transport processes have an important role in morphology evolution, as will be discussed in section 4.2.

Vertically aligned arrays of $SrTiO_3$ nanotubes can be obtained by hydrothermal treatment in $Sr(OH)_2$ solution of titania structures with highly ordered porosity fabricated by the well-known anodization process of titanium plates.[68,139–142] The morphology of the initial titania nanotubes can be controlled by changing the composition of the electrolyte.[142] The as-prepared titania nanotubes are amorphous but can be transformed to anatase by thermal treatment at moderate temperature, fully retaining the ordered structure. Often the hydrothermal conversion is incomplete, with formation of $TiO_2/SrTiO_3$ heterostructures, as will be more extensively discussed in the next section.

The formation of nanoplatelets and nanosheets is promoted by solvothermal synthesis in EG[108,143,144] or by addition of OLA.[145] The morphology and specific surface area (136–156 $m^2\ g^{-1}$) of the product can be controlled by the reactant concentration.[143] Two typical morphologies are shown in Fig. 6b and c.

3.3.4 Heterostructures and superstructures. As anticipated in the previous section, the hydrothermal reaction of titania-

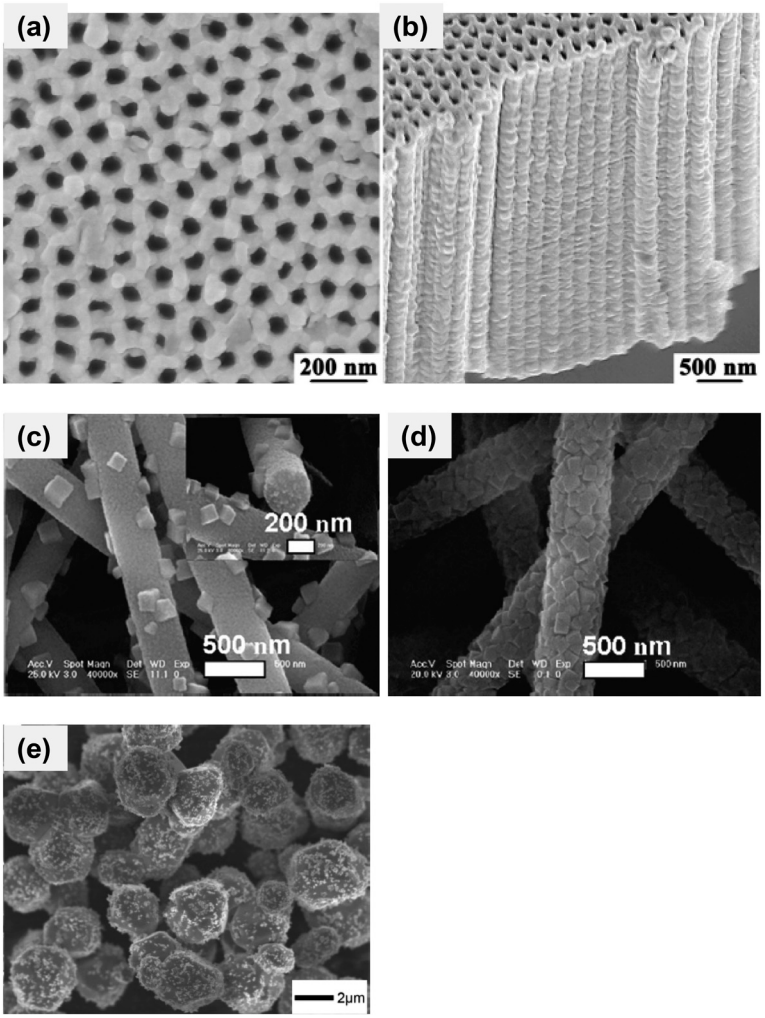

Fig. 8 (a–d) $SrTiO_3/TiO_2$ heterostructures obtained by hydrothermal treatment of different precursors. (a and b) Anatase nanotube array prepared by anodic oxidation of titanium foils (reprinted with permission from Macmillan Publishers Ltd: *Scientific Reports*, ref. 68, copyright 2013), (c and d) anatase fibers prepared by electrospinning (reprinted with permission from ref. 146. Copyright 2011 American Chemical Society). The $Sr(OH)_2$ concentration increases from 1.25×10^{-3} M (c) to 1.25×10^{-2} M (d) while the reaction time (24 h) is kept constant. (e) Ag_3PO_4 particles decorated with $SrTiO_3$ nanocrystals (reprinted with permission from ref. 70. Copyright 2014 American Chemical Society).

based templates with strongly alkaline solutions of Sr salts often proceeds through the heterogeneous nucleation and subsequent growth of perovskite particles on the substrate surface with formation of $TiO_2/SrTiO_3$ heterostructures.[129–131,140,141,146–150] These heterostructures have superior photocatalytic properties in comparison with the pure phases, and this is ascribed to more efficient separation of photogenerated electrons and holes between TiO_2 and $SrTiO_3$.[68,129,147,150] Titania fibres obtained by electrospinning,[146,147] arrays of TiO_2 nanotubes prepared by anodic oxidation of titanium foils[139,140] and $H_2Ti_3O_7$ nanowires resulting from acidic washing of hydrothermally grown $Na_2Ti_3O_7$ nanowires[129] are convenient precursors (Fig. 8a and d). The surface density of perovskite nanocrystals can be controlled by varying the $Sr(OH)_2$ concentration. As shown in Fig. 8c and d, an increase of the concentration from 1.25×10^{-3} M to 1.25×10^{-2} M determines the complete surface coverage. Ordered $TiO_2/SrTiO_3$ nanorod heterostructures can also be prepared by a two-step hydrothermal process.[148] First, vertically aligned nanorods of rutile are grown on a fluorine-doped tin oxide substrate by hydrothermal treatment of an acidic solution of titanium isopropoxide at 150 °C. Then, the resulting nanorod arrays are partially converted into $SrTiO_3$ by reaction with Sr^{2+} ions in an ammonia solution at 180 °C. Core–shell Fe_2O_3@$SrTiO_3$ and $BiFeO_3$@$SrTiO_3$ particles are further examples of composite particles with high photocatalytic activity.[151] Other heterostructures with improved photocatalytic efficiency include $SrTiO_3$–Ag_3PO_4[70] and $SrTiO_3$–MoS_2.[72] In both cases, the photocatalyst is prepared by a two-step hydrothermal process. The $SrTiO_3$ particles are prepared first and then suspended in a solution containing the precursors of the second semiconductor. Hydrothermal treatment of this suspension determines the formation of heterostructures. For example, adhesion of the perovskite nanocrystals on the surface of the bigger (2 μm) Ag_3PO_4 particles is observed for low values of the $SrTiO_3/Ag_3PO_4$ molar ratio, with intimate contact between the two phases (Fig. 8e).

Very recently, composite mesocrystals composed of $BaTiO_3$ and $SrTiO_3$ primary nanocrystals (Fig. 9) were prepared by a two-step solvothermal reaction of hydrogen titanate platelets,[152] first with $Ba(OH)_2$ and then with $Sr(OH)_2$, in mixed water/ethanol mixtures. The second-step treatment can produce either (Ba,Sr)TiO_3 solid solution or composite mesocrystals depending on the solvent composition. The first treatment results in composite $BaTiO_3$-hydrogen titanate mesocrystals.

$SrTiO_3$ hierarchical superstructures with enhanced photocatalytic activity were directly grown on transparent conducting fluorine-doped tin oxide substrates by a combination of chemical bath synthesis and hydrothermal treatment using ZnO microcrystals with a flower-like morphology as initial templates.[153] The morphology and internal structure of the resulting structures could be controlled by varying the hydrothermal reaction temperature (150–200 °C) and time (3–40 h), initial reactant concentration and pH. $SrTiO_3$ hollow

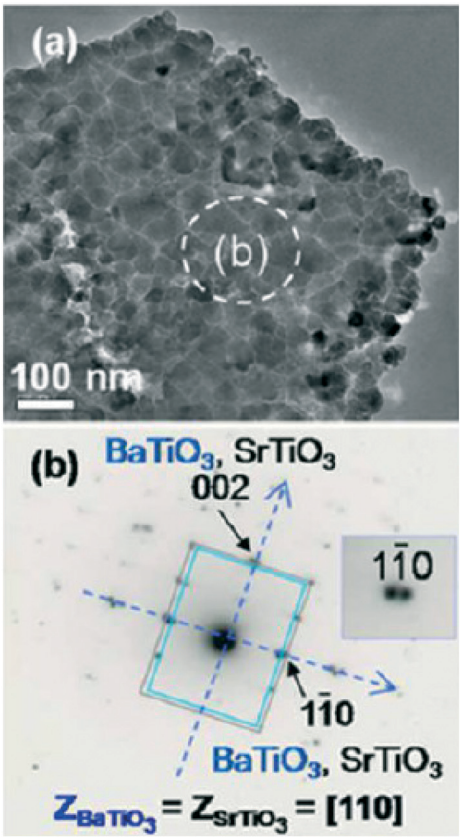

Fig. 9 TEM image (a) and electron diffraction pattern (b) of a $BaTiO_3$–$SrTiO_3$ composite mesocrystal. The splitting of the spots in the ED pattern indicates that the mesocrystal consists of highly oriented nanocrystals of the two perovskites. Reprinted with permission from ref. 152. Copyright 2015 American Chemical Society.

microspheres (diameter: 3–5 μm) composed of randomly oriented nanocubes with an edge of 50–80 nm were hydrothermally synthesised at 180 °C using anatase spherical particles as the precursor and template.[154] The thickness of the shell decreases with increasing reaction time while the size of the primary nanocubes increases. This indicates that the formation of the central cavity is likely determined by an Ostwald ripening process: the inner part of the spherical particles, composed of smaller and more disordered crystallites, is dissolved and re-precipitated in the outer region.

4. Crystallisation mechanisms

The mechanisms of hydrothermal crystallisation of $ATiO_3$ perovskites (A = Ca, Sr, Ba) have been investigated in some detail, especially in the case of $BaTiO_3$. Eckert Jr. *et al.*[155] proposed a general scheme comprising two different crystallisation pathways: *in situ* transformation and dissolution–precipitation. The latter mechanism involves the dissolution of a parent compound and the formation of a new phase by nucleation and molecule- or ion-mediated growth. This reaction path is also supported by a real time neutron scattering investigation.[156] However, the majority of studies

about crystallisation mechanisms are *ex situ* from quenched samples, whereas real time *in situ* experiments are rather scarce, especially if we consider perovskites.[157]

In more recent years, it has been realised that the crystallisation of a compound can also occur according to non-classical pathways by the ordered aggregation or oriented attachment of small nanocrystals in mesocrystals.[120] The three mechanisms will be discussed in detail in the next sections.

4.1 *In situ* transformation

According to *in situ* transformation, the reaction starts on the surface of titania particles and continues by inward diffusion of alkaline-earth and hydroxide ions. However, the term "*in situ* transformation" basically refers to the retention of the particle morphology during the reaction rather than describing a unique and well-defined reaction mechanism. Indeed, the final product can inherit the morphology and sometimes the crystallographic order of the precursor by different reaction pathways. Owing to the very slow ionic mobility in the perovskite lattice at the typical temperatures (<300 °C) adopted in hydrothermal synthesis, the transformation cannot proceed by solid-state diffusion. Rather, *in situ* reaction occurs when highly porous amorphous titania particles are used as precursors, as discussed in section 3.3.2, or when the specific structural characteristics of the precursor compound allows a solvent-mediated topochemical transformation in the final product. Suitable compounds for topochemical manipulation include layered structures in which the interlayer cations are weakly bonded and can be exchanged with cations of similar size,[132] as already anticipated in section 3.3.3. Typically, alkali ions are replaced by protons or alkaline-earth cations. Interesting examples of successful topochemical transformations to perovskites were reported for plate-like hydrogen titanate templates.[152,158,159] However, when the precursor is a layered hydrogen or alkali titanate nanowire, topotactic conversion in $ATiO_3$ is not always observed[84,128–131,137,138] owing to the competition with dissolution and precipitation processes.

4.2 Dissolution–precipitation

In the dissolution–precipitation process, titanium aqueous species ($Ti(OH)_n^{(n-4)-}$) originated from the dissolution of titania or titania-like precursors under highly alkaline conditions are transported through the liquid phase and determine the crystallisation of the perovskite by nucleation (homogeneous nucleation in the liquid phase or heterogeneous nucleation at the surface of a solid substrate) and ion-mediated growth. Alkaline-earth cations usually play a minor role because of the high solubility of the corresponding hydroxides. The overall process can be described by the following reactions:
precursor dissolution:

$$TiO_2(s) + (n-4)OH^-(aq) + 2H_2O(l) \rightarrow Ti(OH)_n^{(n-4)-}(aq) \quad n = 4\text{–}6 \quad (1)$$

perovskite precipitation:

$$Ti(OH)_n^{(n-4)-}(aq) + Sr^{2+}(aq) + (6-n)OH^-(aq) \rightarrow SrTiO_3(s) + 3H_2O \quad (2)$$

A similar reaction can be written for other crystalline titanium precursors. The scheme proposed in ref. 155 is somewhat oversimplified and has been later improved by including other processes which play an important role in crystallisation, such as secondary nucleation and random aggregation.[18,92,160] More recently, the predominant role of heterogeneous nucleation and the tendency of the perovskite to grow on the precursor surface have been clearly shown for the hydrothermal synthesis of $SrTiO_3$ from crystalline precursors with different phase compositions (anatase, rutile, hydrogen titanate, sodium titanate) and morphologies (nanocubes, nanospheres, nanowires, nanosheets).[84,131,149,150,161] This means that reaction (1) (dissolution) and reaction (2) (precipitation) are strongly coupled together in terms of distance (at the nanoscale) between the dissolution and precipitation sites. The coupling is mediated by the solid–liquid interfaces as they play an active role in both dissolution and precipitation. The prevailing heterogeneous nucleation of $SrTiO_3$ on the precursor surface is mainly determined by the large solid–liquid contact surface of the precursor (typically a submicron or nanosized powder), its low solubility and, often, the stagnant fluid state which exists in non-agitated reaction vessels once the reaction temperature has been reached (in the absence of convective transport). Indeed, the hydrothermal treatment is, in many cases, carried out in small (60–125 mL) acid digestion bombs without stirring. Under such conditions, the supply of aqueous titanium species at the reaction site is limited, besides the low precursor solubility and dissolution rate, by the slow diffusional transport, so that the initial formation of the perovskite will be confined in a thin liquid region around the precursor where the supersaturation is high enough. Despite the high supersaturation predicted from thermodynamic calculations (10^7–10^9 for $SrTiO_3$, ref. 84), the bulk of solution remains undersaturated because the majority of the soluble titanium species will be exhausted near the precursor surface. If the dissolution is slow enough, even the effective supersaturation in the interfacial layer will be much lower than that estimated by the thermodynamic calculations and, consequently, the substrate surface will play a significant role in the nucleation. If the product can grow epitaxially on the substrate, the nucleation energy barrier will be strongly reduced. In contrast, without good crystallographic compatibility, nucleation can even become the rate-controlling step. Moreover, in the absence of stirring and convective transport, the precursor particles will settle at the bottom of the reaction vessel, enhancing the role of diffusion.

The morphology evolution after the initial surface nucleation and early growth will be mostly determined by the surface density of nuclei. If the density of the nuclei is high enough, complete surface coverage of the precursor will be

obtained, as observed, for example, in the case of anatase and sodium titanate,[84] and the parent phase will be replaced by the product (Fig. 7b and c), a process known by mineralogists as pseudomorphic transformation, *i.e.*, a different compound takes the place of the parent mineral while preserving the original crystal morphology more or less precisely.[162,163] Transformation of many minerals under hydrothermal conditions was found to occur *via* this kind of replacement reaction.[163–169] Topotactic reactions can be considered as a special case of pseudomorphic transformation. When there is a high degree of structural matching between the perovskite and the precursor as in the case of anatase, the perovskite will grow epitaxially on the substrate in the form of a single crystal or mesocrystal. When there is only a limited substrate/product compatibility, the reaction will lead to a polycrystalline product. According to the heterogeneous nucleation theory, a good crystallographic matching between the substrate and the nucleus significantly reduces the nucleation energy barrier for the formation of the new phase resulting in a faster nucleation, *i.e.* a higher surface density of nuclei.

Although the reaction kinetics will slow down, the replacement reaction will proceed even after complete coverage of the template by the product. Dissolution of the precursor and transport of aqueous species can continue owing to the existence of channels, pores and cracks in the outer product layer, as well documented for pseudomorphic reactions involving dissolutionprecipitation processes.[163,165,167,168] The existence of these defects, especially in the edge regions, is likely because the volume of $SrTiO_3$ formed per unit volume of the parent phase is >1 (1.7 for anatase, 1.9 for rutile, 1.2 for $Na_2Ti_3O_7$). There is some evidence that the transport of soluble species, including titanium hydroxocomplexes, during replacement reactions can occur along pores and channels at grain boundaries and other extended defects.[167,168] The precursor morphology will be more or less precisely retained during the replacement reaction depending on the rate-controlling process. If the transformation is driven by the outward diffusional transport of the titanium aqueous species ($Ti(OH)_n^{(n-4)-}$), the precursor morphology will be loosely retained only at a macroscopic level, as overgrowth will predominate. In this case, the transformation can also result in the development of porous structures or even of hollow structures.[130] Differently, if the precursor dissolution is the controlling step, the initial morphology will be preserved more precisely, as the formation of a new phase will occur at the precursor/product interface.

In contrast, if complete surface coverage is not realised, the morphology evolution will be totally different, as exemplified by the behaviour of $H_2Ti_3O_7$ nanowires.[84] In such a case, the new phase mainly grows as isolated particles with random orientation (Fig. 7a) and a significant fraction of the precursor surface remains uncovered even after 24 h reaction. This indicates that nucleation is more difficult in comparison with other substrates. Due to the incomplete coverage, the precursor morphology is not inherited by the perovskite. Once the precursor relict is exhausted, the perovskite particles are no longer held together.

The heterogeneous nucleation of the perovskite on the substrate surface is likely to prevail even when the precursor is an extremely fine titania powder consisting of particles with a diameter of a few tens of nm. For example, hydrothermal treatment at 220 °C for 20 h of spherical TiO_2 particles with an average diameter of 30 nm resulted in $SrTiO_3$ cubic particles with an average edge length (evaluated from the specific surface area) of 32 nm,[170] which is comparable with the expected value of 29 nm calculated assuming that a single precursor particle transforms in a single perovskite nanocube.

If the duration of the hydrothermal treatment is prolonged after complete transformation and the particles have a relatively broad size distribution and are not stabilized by capping molecules, the average particle size will increase with time due to Ostwald ripening. For example, after hydrothermal treatment at 220 °C for 100 h, the size of $SrTiO_3$ and $BaTiO_3$ cubic nanoparticles increases by a factor of $\approx$1.5.[170,171] However, the coarsening effect can be neglected for short-time treatments. In addition to coarsening, Ostwald ripening can also determine a change in particle morphology[172] towards a crystal shape which minimises the interfacial energy and promote the formation of hollow spheres.[154]

4.3 Non-classical crystallisation and formation of mesocrystals

Analysis of the existing literature concerning the hydrothermal synthesis of $BaTiO_3$ and $SrTiO_3$ indicates that in several cases the crystallisation process cannot be solely described as the nucleation of the new phase and subsequent ion-mediated growth but, rather, by nanoparticle-mediated nonclassical crystallisation. In particular, this happens when the precursor is a freshly or *in situ* prepared gel-like amorphous phase resulting from the rapid hydrolysis of a mixed solution, prepared from soluble Ti and Sr compounds, with a strong base such as NaOH.[84,94,104] As with many other gels, this precursor has an amorphous polymeric network structure with pores and channels with sizes from a few nanometres to a few tens of nanometres filled by the solvent.[95,96] Alkaline-earth ions do not take part in the formation of the network and are adsorbed on the gel or remain in solution. The solvent completely permeates the gel, and there are no well-defined solid surfaces to couple dissolution and precipitation as in the case of crystalline substrates. The huge contact area of the gel network with the solvent and the relatively higher solubility of hydrous amorphous titania (Fig. 3) in comparison with other precursors will produce a higher and homogeneous supersaturation. Consequently, a very large number of small nanocrystals will readily nucleate within the whole gel volume and grow to a limited extent, up to about 5–10 nm. Since the diffusion of the nanocrystals is strongly depressed by the gel network, these nano building units have enough time to reorient under the influence of the

interaction potentials and align along a preferred crystallographic direction, leading to the formation of mesocrystals rather than random aggregates. Reorientation is a fundamental step to remove the free energy barrier to aggregation.[173] In general, gels are well suited for the generation of mesocrystals.[120] TEM and HRTEM observations of $SrTiO_3$ cubic particles obtained by hydrothermal treatment at 200 °C of an AHT precursor prepared from Ti isopropoxide and $Sr(OH)_2$ clearly reveal that they are superstructures that originated from self-assembly of small nanocrystals with sizes of the order of 5 nm[84] (Fig. 10a and b). The existence of steps and terraces on the mesocrystal surface indicates that the growth proceeds layer-by-layer through the oriented attachment of the nano building units at kink and step sites. This process mimics the classical crystal growth mechanism reported in textbooks except that ions and molecules are replaced by nanocrystals. More generally, the morphology of $SrTiO_3$ mesocrystals is highly dependent on the specific precursor, temperature of hydrothermal treatment and solvent composition.

Often, the crystalline subunits of a mesocrystal are in high 3D mutual order resulting in the difficulty to distinguish a mesocrystal from a single crystal, as the mesocrystal shows an identical diffraction pattern and often well-defined external faces (Fig. 10). However, mesocrystals are highly defective owing to (i) the presence of pores and adsorbed organic molecules or polymers (often added to facilitate the oriented aggregation of the primary nanocrystals), (ii) small misalignments between the lattice planes of neighbouring units and (iii) a high density of dislocations. Moreover, the mesocrystal surface appears rough rather than smooth at high magnification. The presence of such features offer the possibility to visualise the primary units and to distinguish a mesocrystal from a single crystal using high resolution electron microscopy, as demonstrated by Fig. 10.

The formation of $SrTiO_3$ mesocrystals by hydrothermal treatment of gel-like precursors is well documented in the literature[84,94,100,104,108,145,174–177] and a couple of studies carefully describe the morphology evolution. Park *et al.*[104] reported the formation of $SrTiO_3$ mesocrystals during hydrothermal treatment in the presence of oleic acid with a Sr/OLA molar ratio of 2. Oleic acid determines the initial growth of nanorods of an intermediate Sr–Ti–O phase and the formation of aggregates in which the primary crystals roughly share a common crystallographic orientation. These aggregates then undergo a process of internal recrystallisation with formation of $SrTiO_3$ mesocrystals composed of cubic subunits first (Fig. 11a and b) and the crystallographic fusion of the subunits in single crystal nanocubes with an irregular surface later (Fig. 11c and d). A high concentration of OLA (Sr/OLA = 0.2) strongly stabilises the initial Sr–Ti–O nanorods and inhibits their transformation in mesocrystals.

A careful investigation on the size and morphology evolution (0.5–600 h) of $SrTiO_3$ particles during hydrothermal synthesis at 140 °C in the presence of PEG has been carried out by Zhan *et al.*[177] Three fundamental crystallisation steps were identified (Fig. 11e): (i) (0.5–24 h) growth of porous spheroidal mesocrystals by oriented aggregation of nano building

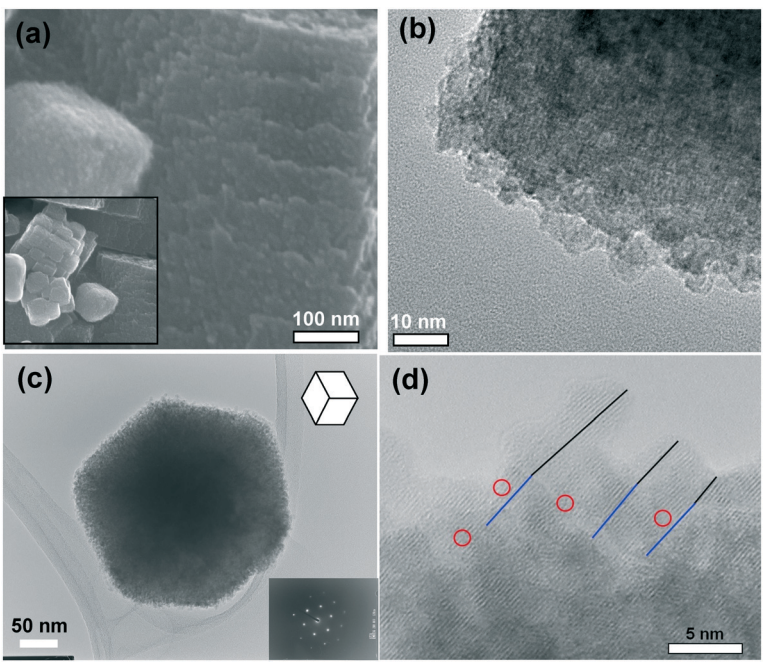

Fig. 10 $SrTiO_3$ cubic mesocrystals obtained by hydrothermal treatment of Sr–Ti gel-like precursors prepared from solutions of (a and b) Ti isopropoxide and $Sr(OH)_2$ (adapted with permission from ref. 84. Copyright 2015 American Chemical Society) and (c and d) $TiOCl_2$ and $SrCl_2$ (adapted with permission from ref. 94. Copyright 2006 American Chemical Society). The images strongly support a non-classical nanocrystal-mediated growth by ordered aggregation of nano building units. The straight lines and circles in (d) indicate small misalignments of the lattice planes and edge dislocations, respectively.

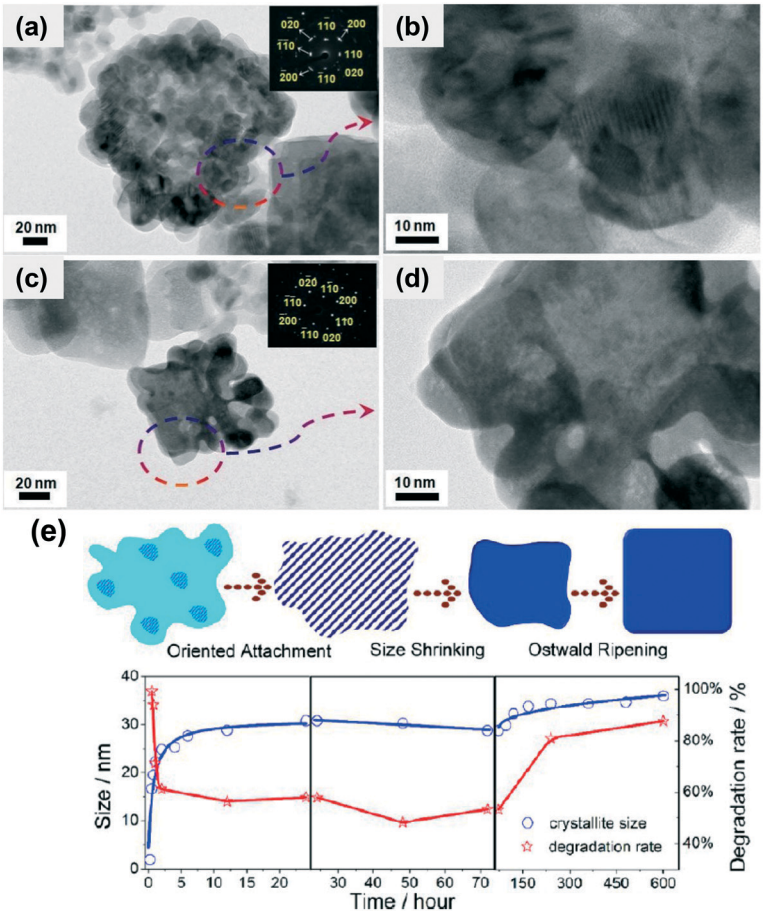

Fig. 11 (a–d) Transformation of $SrTiO_3$ mesocrystals (a and b) in single crystals with an irregular morphology (c and d) by crystallographic fusion during hydrothermal treatment at 240 °C (reproduced from ref. 104 with permission from the Royal Society of Chemistry). (e) Evolution of crystal size and photocatalytic activity of $SrTiO_3$ particles with time during hydrothermal treatment at 140 °C (reprinted with permission from ref. 177. Copyright 2015 American Chemical Society).

units (5 nm). A high density of these primary nanocrystals was identified inside the amorphous precursor after 30 min reaction. (ii) (24–72 h) The mesocrystals undergo a progressive internal rearrangement with crystallographic fusion of the building units and transformation in cubic single crystals. During this process, the particles decrease in size due to the elimination of internal porosity. (iii) (80–600 h). Slow growth and development of well-faceted particles determined by Ostwald ripening. The catalytic activity of $SrTiO_3$ changed significantly depending on the growth stage considered.

Although the presence of specific organic molecules like OLA and PEG which adsorb on the surface of the nanocrystals during the early growth stage is quite effective to drive their oriented aggregation in mesocrystals, the formation of mesocrystals occurs even in the absence of additives.[84,94,131] Calderone *et al.*[94] prepared $SrTiO_3$ mesocrystals under the same experimental conditions either without any additive or by addition of either citric acid or polyacrylic acid. The additive affects both the particle morphology and the degree of alignment of the primary nanocrystals. Without additives, the reaction results in cubic particles with very sharp surfaces composed of building blocks of about 5 nm showing a high degree of crystallographic alignment (Fig. 10c and d). With citric acid, the morphology changes from cubic to spheroidal and the primary nanocrystals are only roughly aligned along the same crystallographic direction. The adsorbed additive molecules remain trapped inside the mesocrystals but can be removed by thermal treatment, leaving a network of nanopores responsible for the high SSA (140 $m^2 g^{-1}$) of the final product.

Hydrothermal treatment of Sr–Ti gel precursors is also suitable for the growth of dendritic $SrTiO_3$ particles.[178–181] It is observed that by decreasing the mineraliser concentration (either NaOH or KOH), the particle morphology evolves from a cuboidal shape to dendritic structures with progressively elongated arms.

5. Defects in hydrothermal perovskites

The most common lattice defects observed in oxides with a perovskite structure obtained by hydrothermal synthesis are represented by hydroxyl groups. The incorporation of water in the perovskite lattice has been extensively investigated in

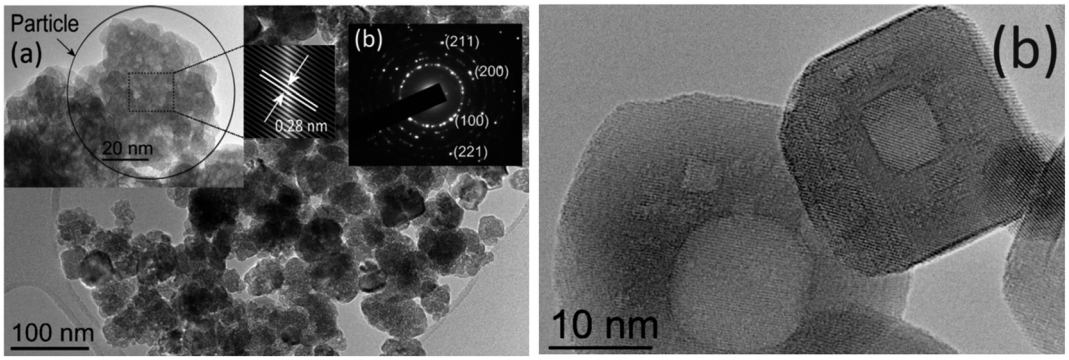

Fig. 12 Two-step hydrothermal synthesis of $SrTiO_3$ particles. The nanocrystal aggregates (a) resulting from hydrothermal reaction at 95 °C (in the inset, their SAED diffraction pattern, see original paper for details) transform into cubic nanocrystals exhibiting internal cavities (b) after hydrothermal crystallisation at 240 °C (reprinted from ref. 176, copyright 2013, with permission from Elsevier).

many acceptor-doped oxides, including alkaline-earth titanates, zirconates, stannates, hafniates, cerates and niobates.[182,183] According to the Kröger–Vink notation, the hydration reaction can be written as

$$H_2O + V_O^{\cdot\cdot} + O_O^x \rightarrow 2OH^{\cdot} \quad (3)$$

where 2 hydroxide ions substitute for 2 oxide ions with the formation of two positively charged $OH^{\cdot}$ defects. Since migration of these species occurs by proton hopping, they are often indicated as proton defects. The concentration of $OH^{\cdot}$ is determined by the water vapour pressure and the oxygen vacancy concentration which, in turn, is controlled by the amount of acceptor dopant (often Y^{3+} at the B site of the perovskite lattice). Because of the high concentration and the high mobility of the protonic defects, acceptor-doped ABO_3 perovskites (A = Ba, Sr and B = Ti, Sn, Zr and Ce) are promising proton conductors for application as electrolytes in SOFCs and hydrogen separation membranes.[182]

Considering that the amount of acceptor impurities in hydrothermally grown oxides, if not intentionally acceptor-doped, is usually very low in comparison with the hydroxyl concentration, the incorporation of $OH^{\cdot}$ defects during the hydrothermal synthesis of perovskites has to occur with a different mechanism from reaction (3). Detailed studies on the incorporation of hydroxyl ions in undoped hydrothermal $ATiO_3$ perovskites and the nature of the corresponding charge compensating defects were mainly carried out for barium titanate,[184–190] although these defects also exist in undoped $SrTiO_3$.[89,176,191,192]

According to Hennings and co-workers,[184,185] the incorporation of hydroxyl groups is compensated by the formation of equal numbers of barium and titanium vacancies $[OH^{\cdot}] = 6[V''_{Ba}] = 6[V''''_{Ti}]$ and, consequently, the chemical formula of hydrothermal $BaTiO_3$ is written as $Ba_{1-(x/6)}(V''_{Ba})_{x/6}Ti_{1-(x/6)}(V''''_{Ti})_{x/6}O_{3-x}(OH^{\cdot})$ where x denotes the fraction of OH groups per defective $BaTiO_3$ formula unit. Existence of a single cation vacancy type would result in a significant deviation from the Ba/Ti = 1 stoichiometry and formation of secondary phases after high temperature calcination. In contrast, single phase and almost stoichiometric powders were obtained.[184,185] In addition, the density of the powders was in good agreement with this defect model. The hydroxyl lattice groups are gradually released in the form of water between 100 and 600 °C. The amount of protons incorporated in the lattice is strongly dependent on synthesis temperature. Powders obtained at low temperature (80–90 °C) show a weight loss of 3–4% between 100 and 800 °C, corresponding to about one water molecule per $BaTiO_3$ formula unit.[189,190] This large amount of defects results in rather low densities, even of the order of 90% of the theoretical $BaTiO_3$ density. In contrast, powders obtained at 250–300 °C release only a small amount of water, usually lower than 1%.[186,190]

TEM observations have revealed that hydrothermally crystallised $SrTiO_3$ particles often show well-faceted internal cavities with circular or square shapes and a size from a few nm to about 10 nm.[176,191–193] The internal faces of the cavities are parallel to the lattice planes. Similar observations were reported for $BaTiO_3$.[194] These nanocavities are rather stable and survive even after thermal treatment at temperatures up to 827 °C. Considering that they are usually observed in particles prepared from gel-like titania or Sr–Ti precursors, their origin is most likely related to the recrystallisation of nanocrystalline aggregates or mesocrystals. Mesocrystals are metastable moieties which undergo, with time or increasing temperature, a process or crystallographic fusion in single crystal particles.[104,120,177] Mesocrystals contain a large amount of small nanopores between the primary nanobuilding blocks and, during the crystallographic fusion, these nanopores coalesce together forming larger cavities. A clear demonstration was given by Setinc *et al.*[176] who synthesised $SrTiO_3$ particles by a two-step process. They first produced nanocrystalline aggregates of $SrTiO_3$ (Fig. 12a) by precipitation at 95 °C from a solution containing $Sr(OH)_2$ and Ti isopropoxide through the addition NaOH. These aggregates transformed into cubic particles with faceted internal cavities by either hydrothermal treatment at 240 °C (Fig. 12b) or annealing at 900 °C. The early

stages of mesocrystal recrystallisation with evidence of nanopore coalescence in larger cavities were also observed after hydrothermal treatment at 200 °C of the gel suspension obtained by the hydrolysis of a solution of $Sr(OH)_2$ and $TiOCl_2$.[84]

6. Conclusions and outlook

The hydrothermal/solvothermal method represents one of the most widely used approaches for the synthesis of a large number of inorganic crystalline compounds under mild conditions. The main advantage of this solution-mediated crystallisation process is the fine control over the composition, morphology and size of the final particles and thus the possibility to produce materials with tailored properties for specific applications. The synthesis of both pure and doped $SrTiO_3$ can be considered as a representative example of the potential of the hydrothermal/solvothermal method, as a large variety of morphologies, from equiaxed (cubes, spheres) to highly anisotropic (rods, wires, platelets) shapes, as well as heterostructures can be obtained by varying some physical and chemical parameters, such as temperature, precursor concentration and nature, solvent and mineraliser composition, stoichiometry and pH. The addition of organic additives with polar groups able to strongly adsorb on the solid surfaces, including surfactants (oleic acid/sodium oleate, CTAB) and hydrophilic polymers (PAA, PVP, PEG), also has a large effect on particle morphology. Molecules like oleic acid and PVP can suppress particle coarsening after the early growth stages, leading to the formation of capped $SrTiO_3$ nanocrystals with a well-defined morphology, a narrow size distribution and an average size even lower than 10 nm. As a result, a solid and widespread know-how on the preparation of high quality fine powders has been achieved.

The nature of the precursor has a fundamental impact on the crystallisation mechanism and morphology of the final product. Often, when an amorphous or gel-like titania precursor is used, self-assembly of primary nanocrystals *via* ordered aggregation or oriented attachment mechanisms leads to the formation of mesocrystals. Some of the above cited organic additives can facilitate the ordered aggregation process. Mesocrystals, owing to the existence of trapped solvent and organic molecules between the primary nanocrystals which determine the formation of a network of pores and channels when these impurities are removed, show high specific surface area and mesoporosity, making them attractive for catalytic and photocatalytic applications. In the case of crystalline precursors, nucleation of $SrTiO_3$ occurs on the precursor surface, and depending on the degree of crystallographic matching, the surface density of nuclei and the rate-controlling process, the hydrothermal reaction can lead to different results. If complete surface coverage of the precursor by the growing $SrTiO_3$ nuclei is rapidly attained, a pseudomorphic transformation retaining more or less precisely the precursor morphology will occur. Both the morphology and crystallographic order will be well preserved in the case of topochemical transformation or epitaxial growth of the product with formation of single crystals or mesocrystals. The retention of the template morphology will be facilitated if the rate-controlling process is the precursor dissolution, as the growth of the new phase will occur at the product/precursor interface. In contrast, if the diffusional transport of the aqueous species generated by the precursor dissolution is predominant, growth will occur at a certain distance from the substrate surface and the initial morphology will be only roughly retained or even lost.

Besides the synthesis of phase pure particles, hydrothermal synthesis is particularly suited for the preparation of heterostructures. The predominant heterogeneous nucleation of $SrTiO_3$ on the surface of crystalline titania or titanate precursors can be exploited to obtain two-phase assemblies with controlled morphology. Again the degree of transformation and the size of the perovskite crystals can be controlled by varying the temperature, concentration and reaction time. The hydrothermal/solvothermal method and, in particular, multistep hydrothermal processes are certainly very promising for realising more complex and efficient heterostructures based on $SrTiO_3$ and other perovskites by controlling the shape, size and connectivity of two or even more crystal phases forming the composite particle as well as the nature of the interfaces. Quite recently, the possibility to prepare composite mesocrystals by a two-step mild hydrothermal process has been demonstrated, opening new perspectives for the fabrication of innovative materials and catalysts.

A further advantage of hydrothermal synthesis is the limited energy consumption arising from the mild temperatures required (in most cases $\leq$250 °C) in comparison with other routes widely used at the industrial level (solid-state reaction, pyrolysis methods, oxalate decomposition, *etc.*). The use of water as a solvent makes the hydrothermal method an environmentally more sustainable process.

Our knowledge about the thermodynamics and the fundamental mechanisms governing the hydrothermal crystallisation of $SrTiO_3$ and, more generally, of ternary inorganic oxides has strongly improved in recent years. Thus, the synthesis process can be better designed to obtain the desired product in a reasonable time avoiding a time consuming trial-and-error approach. Moreover, commercial software is available to predict phase stability diagrams of many inorganic compounds. However, a detailed knowledge of the solution chemistry as well as reliable and complete sets of thermodynamic data for the aqueous species and crystalline phases of a specific system are needed to improve the predictive capabilities. Fortunately, nowadays many *in situ* techniques are available to monitor the crystallisation process (ion-selective sensors and electrodes, spectroscopic methods, X-rays diffraction, *etc.*) and, consequently, the effect of the reaction conditions on the outcome of the reaction can be rapidly mapped and the relevant thermodynamic quantities obtained using regression methods.

Despite the rapid progress of hydrothermal/solvothermal synthesis in recent years, there are still a large number of

opportunities and problems related to this route which have not been explored yet. Some examples include the design of innovative liquid media with specific properties by mixing different solvents, the preparation of new templates and the use of multistep synthesis routes for better morphology and size control, the development of advanced modelling methods which incorporate and couple together both the thermodynamic aspects (solution chemistry, stability of solid phases, yield, *etc.*) and the kinetics of the crystallisation process (nucleation, growth and aggregation rate, evolution of particle size distribution).

References

1 O. A. Marina, N. L. Canfield and J. W. Stevenson, Thermal, electrical, and electrocatalytical properties of lanthanum-doped strontium titanate, *Solid State Ionics*, 2002, **149**, 21.
2 J. H. Haeni, P. Irvin, W. Chang, R. Uecker, P. Reiche, Y. L. Li, S. Choudhury, W. Tian, M. E. Hawley, B. Craigo, A. K. Tagantsev, X. Q. Pan, S. K. Streiffer, L. Q. Chen, S. W. Kirchoefer, J. Levy and D. G. Schlom, Room-temperature ferroelectricity in strained $SrTiO_3$, *Nature*, 2004, **430**, 758.
3 A. Kudo and Y. Miseri, Heterogeneous photocatalyst materials for water splitting, *Chem. Soc. Rev.*, 2009, **38**, 253.
4 M. S. Wrighton, A. B. Ellis, P. T. Wolczanski, D. L. Morse, H. B. Abrahamson and D. S. Ginley, Strontium titanate photoelectrodes. Efficient photoassisted electrolysis of water at zero applied potential, *J. Am. Chem. Soc.*, 1976, **98**, 2774.
5 G. Shirane and Y. Yamada, Lattice-Dynamical Study of the 110 K Phase Transition in $SrTiO_3$, *Phys. Rev.*, 1969, **177**, 858.
6 P. I. Cowin, C. T. G. Petit, R. Lan, J. T. S. Irvine and S. Tao, Recent progress in the development of anode materials for solid oxide fuel cells, *Adv. Energy Mater.*, 2011, **1**, 314.
7 T. Puangpetch, T. Sreethawong, S. Yoshikawa and S. Chavadej, Synthesis and photocatalytic activity in methyl orange degradation of mesoporous-assembled $SrTiO_3$ nanocrystals prepared by sol–gel method with the aid of structure-directing surfactant, *J. Mol. Catal. A: Chem.*, 2008, **287**, 70.
8 H. Yu, S. X. Ouyang, S. C. Yan, Z. S. Li, T. Yu and Z. G. Zou, Sol-gel hydrothermal synthesis of visible-light-driven Cr-doped $SrTiO_3$ for efficient hydrogen production, *J. Mater. Chem. A*, 2011, **21**, 11347.
9 P. Balaya, M. Ahrens, L. Kienle, J. Maier, B. Rahmati, S. B. Lee and W. Sigle, Synthesis and characterization of nanocrystalline $SrTiO_3$, *J. Am. Ceram. Soc.*, 2006, **89**, 2804.
10 M. Kakihana, T. Okubo, M. Arima, Y. Nakamura, M. Yashima and M. Yoshimura, Polymerized Complex Route to the Synthesis of Pure SrTiO3 at Reduced Temperatures: Implication for Formation of Sr-Ti Heterometallic Citric Acid Complex, *J. Sol-Gel Sci. Technol.*, 1998, **12**, 95.
11 V. Subramanian, R. K. Roeder and E. E. Wolf, Synthesis and UV-Visible-Light Photoactivity of Noble-Metal-$SrTiO_3$ Composites, *Ind. Eng. Chem. Res.*, 2006, **45**, 2187.
12 Y. B. Mao, S. Banerjee and S. S. Wong, Large-scale synthesis of single crystalline perovskite nanostructures, *J. Am. Chem. Soc.*, 2003, **125**, 15718.
13 D. Grosso, C. Boissiere, B. Smarsly, T. Brezesinski, N. Pinna, P. A. Albouy, H. Amenitsch, M. Antonietti and C. Sanchez, Periodically ordered nanoscale islands and mesoporous films composed of nanocrystalline multimetallic oxides, *Nat. Mater.*, 2004, **3**, 787.
14 X. Fan, Y. Wang, X. Chen, L. Gao, W. Luo, Y. Yuan, Z. Li, T. Yu, J. Zhu and Z. Zou, Facile method to synthesize mesoporous multimetal oxides ($ATiO_3$, A = Sr, Ba) with large specific surface areas and crystalline pore walls, *Chem. Mater.*, 2010, **22**, 1276.
15 J. Wang, S. Yin, Q. Zhang, F. Saito and T. Sato, Mechanochemical synthesis of $SrTiO_{3-x}F_x$ with high visible light photocatalytic activities for nitrogen monoxide destruction, *J. Mater. Chem.*, 2003, **13**, 2348.
16 J. Poth, R. Haberkorn and H. P. Beck, Combustion-synthesis of $SrTiO_3$ - Part I. Synthesis and properties of the ignition products, *J. Eur. Ceram. Soc.*, 2000, **20**, 707.
17 F. Zou, Z. Jiang, X. Qin, Y. Zhao, L. Jiang, J. Zhi, T. Xiao and P. P. Edwards, Template-free synthesis of mesoporous N-doped $SrTiO_3$ perovskite with high visible-light-driven photocatalytic activity, *Chem. Commun.*, 2012, **48**, 8514.
18 D. R. Modeshia and R. I. Walton, Solvothermal synthesis of perovskites and pyrochlores: crystallisation of functional oxides under mild conditions, *Chem. Soc. Rev.*, 2010, **39**, 4303.
19 T. K. Townsend, N. D. Browning and F. E. Osterloh, Nanoscale Strontium Titanate Photocatalysts for Overall Water Splitting, *ACS Nano*, 2012, **6**, 742.
20 R. Niishiro, S. Tanaka and A. Kudo, Hydrothermal-synthesized $SrTiO_3$ photocatalyst codoped with rhodium and antimony with visible-light response for sacrificial H_2 and O_2 evolution and application to overall water splitting, *Appl. Catal., B*, 2014, **150–151**, 18.
21 K. A. Müller and H. Burkard, $SrTiO_3$: An intrinsic quantum paraelectric below 4 K, *Phys. Rev. B: Condens. Matter Mater. Phys.*, 1979, **19**, 359.
22 J. G. Bednorz and K. A. Müller, $Sr_{1-x}Ca_xTiO_3$: An XY quantum ferroelectric with transition to randomness, *Phys. Rev. Lett.*, 1984, **52**, 228.
23 C. Ang, Z. Yu, P. M. Vilarinho and J. L. Baptista, Bi:$SrTiO_3$: A quantum ferroelectric and a relaxor, *Phys. Rev. B: Condens. Matter Mater. Phys.*, 1998, **57**, 740.
24 M. Itoh, R. Wang, Y. Inaguma, T. Yamaguchi, Y.-J. Shan and T. Nakamura, Ferroelectricity Induced by Oxygen Isotope Exchange in Strontium Titanate Perovskite, *Phys. Rev. Lett.*, 1999, **82**, 354.
25 H. Ewe and T. Sakudo, Stress-induced ferroelectricity and soft phonon modes in $SrTiO_3$, *Phys. Rev. B: Solid State*, 1976, **13**, 271.
26 V. V. Shvartsman, S. Bedanta, P. Borisov and W. Kleemann, (Sr;Mn)TiO_3: A Magnetoelectric Multiglass, *Phys. Rev. Lett.*, 2008, **101**, 165704.

27 P. Zubko, G. Catalan, A. Buckley, P. R. L. Welche and J. F. Scott, Strain-Gradient-Induced Polarization in $SrTiO_3$ Single Crystals, *Phys. Rev. Lett.*, 2007, **99**, 167601.
28 A. K. Tagantsev, V. O. Sherman, K. F. Astafiev, J. Venkatesh and N. J. Setter, Ferroelectric materials for microwave tunable applications, *J. Electroceram.*, 2003, **11**, 5.
29 D. Fuchs, C. W. Schneider, R. Schneider and H. Rietschel, High dielectric constant and tunability of epitaxial $SrTiO_3$ thin film capacitors, *J. Appl. Physiol.*, 1999, **85**, 7362.
30 P. Kužel, F. Kadlec, H. Němec, R. Ott, E. Hollmann and N. Klein, Dielectric tunability of $SrTiO_3$ thin films in the terahertz range, *Appl. Phys. Lett.*, 2006, **88**, 102901.
31 Q. W. Zhang, J. W. Zhai and L. B. Kong, Relaxor Ferroelectric Materials for Microwave Tunable Applications, *J. Adv. Dielectr.*, 2012, **1**, 1230002.
32 W. T. Chang and L. Sengupta, MgO-mixed $Ba_{0.6}Sr_{0.4}TiO_3$ bulk ceramics and thin films for tunable microwave applications, *J. Appl. Physiol.*, 2002, **92**, 3941.
33 U. C. Chung, C. Elissalde, M. Maglione, C. Estournès, M. Paté and J. P. Ganne, Low-losses, highly tunable $Ba_{0.6}Sr_{0.4}TiO_3$/MgO composite, *Appl. Phys. Lett.*, 2008, **92**, 042902.
34 N. Yamaoka and M. Tetsuo, Properties of $SrTiO_3$-based boundary layer capacitors, *Adv. Ceram.*, 1981, **1**, 232.
35 J. Klekk and P. J. H. Sanders, $SrTiO_3$ boundary layer capacitors: influence of additives and stoichiometry, *Adv. Ceram.*, 1981, **1**, 282.
36 O. N. Tufte and P. W. Chapman, Electron mobility in semiconducting strontium titanate, *Phys. Rev.*, 1967, **155**, 796.
37 T. Okuda, K. Nakanishi, S. Miyasaka and Y. Tokura, Large thermoelectric response of metallic perovskites: $Sr_{1-x}La_xTiO_3$ ($0 \leq x \leq 0.1$), *Phys. Rev. B: Condens. Matter Mater. Phys.*, 2001, **63**, 113104.
38 S. Ohta, T. Nomura, H. Ohta and K. Koumoto, High-temperature carrier transport and thermoelectric properties of heavily La- or Nb-doped $SrTiO_3$ single crystals, *J. Appl. Phys.*, 2005, **97**, 034106.
39 J. Son, P. Moetakef, B. Jalan, O. Bierwagen, N. J. Wright, R. Engel-Herbert and S. Stemmer, Epitaxial $SrTiO_3$ films with electron mobilities exceeding 30,000 $cm^2\ V^{-1}\ s^{-1}$, *Nat. Mater.*, 2010, **9**, 482.
40 P. R. Slater, D. P. Fagg and J. T. S. Irvine, Synthesis and electrical characterisation of doped perovskite titanates as potential anode materials for solid oxide fuel cells, *J. Mater. Chem.*, 1997, **7**, 2495.
41 S. Q. Hui and A. Petric, Evaluation of yttrium-doped $SrTiO_3$ as an anode for solid oxide fuel cells, *J. Eur. Ceram. Soc.*, 2002, **22**, 1673.
42 D. Neagu and J. T. S. Irvine, Structure and Properties of $La_{0.4}Sr_{0.4}TiO_3$ Ceramics for Use as Anode Materials in Solid Oxide Fuel Cells, *Chem. Mater.*, 2010, **22**, 5042–5053.
43 I. Denk, W. Munch and J. Maier, Partial conductivities in $SrTiO_3$: Bulk polarization experiments, oxygen concentration cell measurements, and defect-chemical modeling, *J. Am. Ceram. Soc.*, 1995, **78**, 3265.
44 A. Rothschild, W. Menesklou, H. L. Tuller and E. Ivers-Tiffée, Electronic Structure, Defect Chemistry, and Transport Properties of $SrTi_{1-x}Fe_xO_{3-y}$ Solid Solutions, *Chem. Mater.*, 2006, **18**, 3651.
45 J. R. Jurado, F. M. Figueiredo, B. Gharbage and J. R. Frade, Electrochemical permeability of $Sr_{0.7}$(Ti, Fe)$O_{3-\delta}$ materials, *Solid State Ionics*, 1999, **118**, 89.
46 J. W. Fergus, Oxide materials for high temperature thermoelectric energy conversion, *J. Eur. Ceram. Soc.*, 2012, **32**, 525.
47 K. Koumoto, Y. F. Wang, R. Z. Zhang, A. Kosuga and R. Funahashi, Oxide thermoelectric materials: a nanostructuring approach, *Annu. Rev. Mater. Res.*, 2010, **40**, 363.
48 S. Lee, G. Yang, R. H. T. Wilke, S. Trolier-McKinstry and C. A. Randall, Thermopower in highly reduced n-type ferroelectric and related perovskite oxides and the role of heterogeneous nonstoichiometry, *Phys. Rev. B: Condens. Matter Mater. Phys.*, 2009, **79**, 134110.
49 H. Ohta, S. Kim, Y. Mune, T. Mizoguchi, K. Nomura, S. Ohta, T. Nomura, Y. Nakanishi, Y. Ikuhara, M. Hirano, H. Hosono and K. Koumoto, Giant thermoelectric Seebeck coefficient of a two-dimensional electron gas in $SrTiO_3$, *Nat. Mater.*, 2007, **6**, 129.
50 I. Pallecchi, F. Telesio, D. Li, A. Fête, S. Gariglio, J.-M. Triscone, A. Filippetti, P. Delugas, V. Fiorentini and D. Marré, Giant oscillating thermopower at oxide interfaces, *Nat. Commun.*, 2015, **6**, 6678.
51 Y. Watanabe, J. G. Bednorz, A. Bietsch, Ch. Gerber, D. Widmer, A. Beck and S. J. Wind, Current-driven insulator–conductor transition and nonvolatile memory in chromium doped $SrTiO_3$ single crystals, *Appl. Phys. Lett.*, 2001, **78**, 3738.
52 E. Bellingeri, L. Pellegrino, D. Marré, I. Pallecchi and A. S. Siri, All-$SrTiO_3$ field effect devices made by anodic oxidation of epitaxial semiconducting thin films, *Appl. Phys. Lett.*, 2003, **94**, 5976.
53 K. Szot, W. Speier, G. Bihlmayer and R. Waser, Switching the electrical resistance of individual dislocations in single-crystalline $SrTiO_3$, *Nat. Mater.*, 2006, **5**, 312.
54 M. Janousch, G. I. Meijer, U. Staub, B. Delley, S. F. Karg and B. P. Andreasson, Role of oxygen vacancies in Cr-doped $SrTiO_3$ for resistance-change memory, *Adv. Mater.*, 2007, **19**, 2232.
55 K. Van Benthema and C. Elsässer, Bulk electronic structure of $SrTiO_3$: Experiment and theory, *J. Appl. Phys.*, 2001, **90**, 6156.
56 R. Moos and K. H. Härdtl, Defect chemistry of donor-doped and undoped strontium titanate ceramics between 1000°C and 1400°C, *J. Am. Ceram. Soc.*, 1997, **80**, 2549.
57 A. Ohtomo and H. Y. Hwang, A high-mobility electron gas at the $LaAlO_3/SrTiO_3$ heterointerface, *Nature*, 2004, **427**, 424.
58 A. Fujishima and K. Honda, Electrochemical Photolysis of Water at a Semiconductor Electrode, *Nature*, 1972, **238**, 37.
59 K. Domen, S. Naito, T. Onishi, K. Tamaru and M. J. Soma, Study of the photocatalytic decomposition of water vapor

over a nickel(II) oxide-strontium titanate ($SrTiO_3$) catalyst, *J. Phys. Chem.*, 1982, **86**, 3657.

60 T. K. Townsend, N. D. Browning and F. E. Osterloh, Overall photocatalytic water splitting with NiO_x–$SrTiO_3$ – a revised mechanism, *Energy Environ. Sci.*, 2012, **5**, 9543.

61 R. Konta, T. Ishii, H. Kato and A. J. Kudo, Photocatalytic Activities of Noble Metal Ion Doped $SrTiO_3$ under Visible Light Irradiation, *J. Phys. Chem. B*, 2004, **108**, 8992.

62 T. Ishii, H. Kato and A. Kudo, H_2 evolution from an aqueous methanol solution on $SrTiO_3$ photocatalysts codoped with chromium and tantalum ions under visible light irradiation, *J. Photochem. Photobiol., A*, 2004, **163**, 181.

63 H. Kato and A. Kudo, Visible-Light-Response and Photocatalytic Activities of TiO_2 and $SrTiO_3$ Photocatalysts Codoped with Antimony and Chromium, *J. Phys. Chem. B*, 2002, **106**, 5029.

64 R. Niishiro, H. Kato and A. Kudo, Nickel and either tantalum or niobium-codoped TiO_2 and $SrTiO_3$ photocatalysts with visible-light response for H_2 or O_2 evolution from aqueous solutions, *Phys. Chem. Chem. Phys.*, 2005, **7**, 2241.

65 T. Ohno, T. Tsubota, Y. Nakamura and K. Sayama, Preparation of S, C cation-codoped $SrTiO_3$ and its photocatalytic activity under visible light, *Appl. Catal., A*, 2005, **288**, 74.

66 T.-H. Xie, X. Sun and J. Lin, Enhanced Photocatalytic Degradation of RhB Driven by Visible Light-Induced MMCT of Ti(IV)-O-Fe(II) Formed in Fe-Doped $SrTiO_3$, *J. Phys. Chem. C*, 2008, **112**, 9753.

67 T. Arai, S. Sato, T. Kajino and T. Morikawa, Solar CO_2 reduction using H_2O by a semiconductor/metal-complex hybrid photocatalyst: enhanced efficiency and demonstration of a wireless system using $SrTiO_3$ photoanodes, *Energy Environ. Sci.*, 2013, **6**, 1274.

68 Z. Jiao, T. Chen, J. Xiong, T. Wang, G. Lu, J. Ye and Y. Bi, Visible-light-driven photoelectrochemical and photocatalytic performances of Cr-doped $SrTiO_3$/TiO_2 heterostructured nanotube arrays, *Sci. Rep.*, 2013, **3**, 2720.

69 J. Guo, S. Ouyang, P. Li, Y. Zhang, T. Kako and J. Ye, A new heterojunction Ag_3PO_4/Cr-$SrTiO_3$ photocatalyst towards efficient elimination of gaseous organic pollutants under visible light irradiation, *Appl. Catal., B*, 2013, **134–135**, 286.

70 X. Guan and L. Guo, Cocatalytic Effect of $SrTiO_3$ on Ag_3PO_4 toward Enhanced Photocatalytic Water Oxidation, *ACS Catal.*, 2014, **4**, 3020.

71 Y. Jia, S. Shen, D. Wang, X. Wang, J. Shi, F. Zhang, H. Han and C. Li, Composite Sr_2TiO_4/$SrTiO_3$(La,Cr) heterojunction based photocatalyst for hydrogen production under visible light irradiation, *J. Mater. Chem. A*, 2013, **1**, 7905.

72 J. Liu, L. Zhang, N. Li, Q. Tian, J. Zhou and Y. Sun, Synthesis of MoS_2/$SrTiO_3$ composite materials for enhanced photocatalytic activity under UV irradiation, *J. Mater. Chem. A*, 2015, **3**, 706.

73 S. Burnside, J.-E. Moser, K. Brooks, M. Grätzel and D. Cahen, Nanocrystalline Mesoporous Strontium Titanate as Photoelectrode Material for Photosensitized Solar Devices: Increasing Photovoltage through Flatband Potential Engineering, *J. Phys. Chem. B*, 1999, **103**, 9328.

74 A. Rabenau, The Role of Hydrothermal Synthesis in Preparative Chemistry, *Angew. Chem., Int. Ed. Engl.*, 1985, **24**, 1026.

75 C. S. Cundy and P. A. Cox, The Hydrothermal Synthesis of Zeolites: History and Development from the Earliest Days to the Present Time, *Chem. Rev.*, 2003, **103**, 663.

76 K. Byrappa and T. Adschiri, Hydrothermal technology for nanotechnology, *Prog. Cryst. Growth Charact. Mater.*, 2007, **53**, 117.

77 W. Shi, S. Song and H. Zhang, Hydrothermal synthetic strategies of inorganic semiconducting nanostructures, *Chem. Soc. Rev.*, 2013, **42**, 5714.

78 L. Y. Liang, X. L. Kang, Y. H. Sang and H. Liu, One-Dimensional Ferroelectric Nanostructures: Synthesis, Properties, and Applications, *Adv. Sci.*, 2016, **3**, 1500358.

79 J. Guo, H. Guo, A. L. Baker, M. T. Lanagan, E. R. Kupp, G. L. Messing and C. A. Randall, Cold Sintering: A Paradigm Shift for Processing and Integration of Ceramics, *Angew. Chem., Int. Ed.*, 2016, **55**, 11457.

80 J. Guo, S. S. Berbano, H. Guo, A. L. Baker, M. T. Lanagan and C. A. Randall, Cold Sintering Process of Composites: Bridging the Processing Temperature Gap of Ceramic and Polymer Materials, *Adv. Funct. Mater.*, 2016, **26**, 7115.

81 M. M. Lencka and R. E. Riman, Thermodynamic modeling of hydrothermal synthesis of ceramic powders, *Chem. Mater.*, 1993, **5**, 61.

82 M. M. Lencka and R. E. Riman, Thermodynamics of the hydrothermal synthesis of calcium titanate with reference to other alkaline-earth titanates, *Chem. Mater.*, 1995, **7**, 18.

83 M. M. Lencka and R. E. Riman, Hydrothermal synthesis of perovskite materials: thermodynamic modeling and experimental verification, *Ferroelectrics*, 1994, **151**, 159.

84 V. Kalyani, B. S. Vasile, A. Ianculescu, A. Testino, A. Carino, M. T. Buscaglia, V. Buscaglia and P. Nanni, Hydrothermal Synthesis of $SrTiO_3$: Role of Interfaces, *Cryst. Growth Des.*, 2015, **15**, 5712.

85 K. G. Knauss, M. J. Dibley, W. L. Bourcier and H. F. Shaw, Ti(IV) hydrolysis constants derived from rutile solubility measurements made from 100 to 300°C, *Appl. Geochem.*, 2001, **16**, 1115.

86 J. Schmidt and W. J. Vogelsberger, Aqueous Long-Term Solubility of Titania Nanoparticles and Titanium(IV) Hydrolysis in a Sodium Chloride System Studied by Adsorptive Stripping Voltammetry, *J. Solution Chem.*, 2009, **38**, 1267.

87 T. Sugimoto, X. Zhou and A. J. Muramatsu, Synthesis of Uniform Anatase TiO_2 Nanoparticles by Gel–Sol Method 1. Solution Chemistry of $Ti(OH)_n^{(4-n)+}$ Complexes, *J. Colloid Interface Sci.*, 2002, **252**, 339.

88 A. V. Kostrikin, F. M. Spiridonov, I. V. Lin'ko, B. E. Zaitsev, O. V. Kosenkova, S. V. Tarasova and L. N. Komissarova, Russ., Interaction of Components in the $NaOH–TiO_2 \cdot H_2O–H_2O$ System at 25°C, *Russ. J. Inorg. Chem.*, 2011, **56**, 928.

89 S. Ahuja and T. R. N. Kutty, Nanoparticles of $SrTiO_3$ prepared by gel to crystallite conversion and their

photocatalytic activity in the mineralization of phenol, *J. Photochem. Photobiol., A*, 1996, **97**, 99.

90 V. Kumar, Solution-precipitation of fine powders of barium titanate and strontium titanate, *J. Am. Ceram. Soc.*, 1999, **82**, 2580.

91 S. Zhang, Y. Han, B. Chen and X. Song, The influence of TiO_2*H_2O gel on hydrothermal synthesis of $SrTiO_3$ powders, *Mater. Lett.*, 2001, **51**, 368.

92 S. C. Zhang, J. X. Liu, Y. X. Han, B. C. Chen and X. G. Li, Formation mechanisms of $SrTiO_3$ nanoparticles under hydrothermal conditions, *Mater. Sci. Eng., B*, 2004, **110**, 11.

93 D. Chen, X. Jiao and M. Zhang, Hydrothermal synthesis of strontium titanate powders with nanometer size derived from different precursors, *J. Eur. Ceram. Soc.*, 2000, **20**, 1261.

94 V. R. Calderone, A. Testino, M. T. Buscaglia, M. Bassoli, C. Bottino, M. Viviani, V. Buscaglia and P. Nanni, Size and Shape Control of $SrTiO_3$ Particles Grown by Epitaxial Self-Assembly, *Chem. Mater.*, 2006, **18**, 1627.

95 D. Hennings, G. Rosenstein and H. J. Schreinemacher, Hydrothermal preparation of barium titanate from barium-titanium acetate gel precursors, *J. Eur. Ceram. Soc.*, 1991, **8**, 107.

96 I. Mac Laren and C. B. Ponton, A TEM and HREM study of particle formation during barium titanate synthesis in aqueous solution, *J. Eur. Ceram. Soc.*, 2000, **20**, 1267.

97 K. Huang, L. Yuan and S. Feng, Crystal facet tailoring arts in perovskite oxides, *Inorg. Chem. Front.*, 2015, **2**, 965.

98 R. I. Eglitis and D. Vanderbilt, First-principles calculations of atomic and electronic structure of $SrTiO_3$ (001) and (011) surfaces, *Phys. Rev. B: Condens. Matter Mater. Phys.*, 2008, **7**, 195408.

99 T. Sano, D. M. Saylor and G. S. Rohrer, Surface energy enisotropy of $SrTiO_3$ at 1400°C in air, *J. Am. Ceram. Soc.*, 2003, **86**, 1933.

100 F. Dang, K.-I. Mimura, K. Kato, H. Imai, S. Wada, H. Haneda and M. Kuwabara, Growth of monodispersed $SrTiO_3$ nanocubes by thermohydrolysis method, *CrystEngComm*, 2011, **13**, 3878.

101 U. Sulaemana, S. Yin and T. Sato, Solvothermal synthesis and photocatalytic properties of chromium-doped $SrTiO_3$ nanoparticles, *Appl. Catal., B*, 2011, **105**, 206.

102 K. Park, J. S. Son, S. I. Woo, K. Shin, M.-W. Oh, S.-D. Park and T. Hyeon, Colloidal synthesis and thermoelectric properties of La-doped $SrTiO_3$ nanoparticles, *J. Mater. Chem. A*, 2014, **2**, 4217.

103 L. Hu, C. Wang, S. Lee, R. E. Winans, L. D. Marks and K. R. Poeppelmeier, $SrTiO_3$ nanocuboids from a lamellar microemulsion, *Chem. Mater.*, 2013, **25**, 378.

104 N.-H. Park, Y. Wang, W.-S. Seo, F. Dang, C. Wana and K. Koumoto, Solution synthesis and growth mechanism of $SrTiO_3$ mesocrystals, *CrystEngComm*, 2013, **15**, 679.

105 Y. Hao, X. Wang and L. Li, Highly dispersed $SrTiO_3$ nanocubes from a rapid sol-precipitation method, *Nanoscale*, 2014, **6**, 7940.

106 M. Niederberger, G. Garnweitner, N. Pinna and M. Antonietti, Nonaqueous and halide-free route to crystalline $BaTiO_3$, $SrTiO_3$, and (Ba,Sr)TiO_3 nanoparticles via a mechanism involving C-C bond formation, *J. Am. Chem. Soc.*, 2004, **126**, 9120.

107 L. Dong, H. Shi, K. Cheng, Q. Wang, W. Weng and W. Han, Shape-controlled growth of $SrTiO_3$ polyhedral submicro/nanocrystals, *Nano Res.*, 2014, **7**, 1311.

108 T. Kimijima, K. Kanie, M. Nakaya and A. Muramatsu, Solvothermal synthesis of $SrTiO_3$ nanoparticles precisely controlled in surface crystal planes and their photocatalytic activity, *Appl. Catal., B*, 2014, **144**, 462.

109 G. Xu, Z. Tao, Y. Zhao, Y. Zhang, Z. Ren, G. Shen, G. Han and X. Wei, Solvothermal synthesis, characterization and formation mechanism of single-crystalline $SrTiO_3$ dense spheres with monoethanolamine as reaction medium solvent, *CrystEngComm*, 2013, **15**, 1439.

110 J. Y. Choi, C. H. Kim and D. K. Kim, Hydrothermal Synthesis of spherical perovskite oxide powders using spherical gel powders, *J. Am. Ceram. Soc.*, 1998, **8**, 1353.

111 Y. Wang, H. Xu, X. Wang, X. Zhang, H. Jia, L. Zhang and J. Qiu, A general approach to porous crystalline TiO_2, $SrTiO_3$, and $BaTiO_3$ spheres, *J. Phys. Chem. B*, 2006, **110**, 13835.

112 X. Wei, G. Xu, Z. Ren, Y. Wang, G. Shen and G. Han, Synthesis and characterization of mesoporous $SrTiO_3$ spheres via a poly vinyl alcohol-assisted hydrothermal route, *J. Am. Ceram. Soc.*, 2008, **91**, 299.

113 X. Wei, G. Xu, Z. Ren, C. Xu, W. Weng, G. Shen and G. Han, Single-crystal-like mesoporous $SrTiO_3$ spheres with enhanced photocatalytic performance, *J. Am. Ceram. Soc.*, 2010, **93**, 1297.

114 A. F. Demirörs and A. Imhof, $BaTiO_3$, $SrTiO_3$, $CaTiO_3$, and $Ba_xSr_{1-x}TiO_3$ Particles: A General Approach for Monodisperse Colloidal Perovskites, *Chem. Mater.*, 2009, **21**, 3002.

115 Q. Kuang and S. Yang, Template Synthesis of single-crystal-like porous $SrTiO_3$ nanocube assemblies and their enhanced photocatalytic hydrogen evolution, *ACS Appl. Mater. Interfaces*, 2013, **5**, 3683.

116 P. Jayabal, V. Sasirekha, J. Mayandi, K. Jeganathan and V. Ramakrishnan, A facile hydrothermal synthesis of $SrTiO_3$ for dye sensitized solar cell application, *J. Alloys Compd.*, 2014, **586**, 456.

117 H. Yu, S. Ouyang, S. Yan, Z. Li, T. Yu and Z. Zou, Sol–gel hydrothermal synthesis of visible-light-driven Cr-doped $SrTiO_3$ for efficient hydrogen production, *J. Mater. Chem.*, 2011, **21**, 11347.

118 Y. Zhang, G. Xu, X. Wei, Z. Ren, Y. Liu, G. Shen and G. Han, Hydrothermal synthesis, characterization and formation mechanism of self-assembled mesoporous $SrTiO_3$ spheres assisted with Na_2SiO_3*$9H_2O$, *CrystEngComm*, 2012, **14**, 3702.

119 G. Xu, S. Deng, Y. Zhang, X. Wei, X. Yang, Y. Liu, G. Shen and G. Han, Mesoporous-structure-tailored hydrothermal synthesis and mechanism of the $SrTiO_3$ mesoporous spheres by controlling the silicate semipermeable membranes with the KOH concentrations, *CrystEngComm*, 2014, **16**, 2025.

120 R.-Q. Song and H. Cölfen, Mesocrystals-Ordered Nanoparticles Superstructures, *Adv. Mater.*, 2010, **22**, 1301.
121 V. Buscaglia and M. T. Buscaglia, Synthesis and Properties of Ferroelectric Nanotubes and Nanowires: A Review, in *Nanoscale Ferroelectrics and Multiferroics: Key Processing and Characterization Issues, and Nanoscale Effects*, ed. M. Algueró, J. M. Gregg and L. Mitoseriu, John Wiley & Sons, 2016.
122 U. A. Joshi and J. S. Lee, Template-free hydrothermal synthesis of single crystalline barium titanate and strontium titanate nanowires, *Small*, 2005, **1**, 1172.
123 J. J. Urban, W. S. Yun, Q. Gu and H. Park, Synthesis of Single-Crystalline Perovskite Nanorods Composed of Barium Titanate and Strontium Titanate, *J. Am. Chem. Soc.*, 2002, **124**, 1186.
124 Y. B. Mao, S. Banerjee and S. S. Wong, Hydrothermal synthesis of perovskite nanotubes, *Chem. Commun.*, 2003, 408.
125 Y. Jing, S. Jin, Y. Z. Jia, J. D. Han and J. H. Sun, Preparation of $SrTiO_3$ nanofibres by hydrothermal method, *J. Mater. Sci.*, 2005, **40**, 6315.
126 J. Wang, S. Yin and T. Sato, Characterization and evaluation of fibrous $SrTiO_3$ prepared by hydrothermal process for the destruction of NO, *J. Photochem. Photobiol., A*, 2007, **187**, 72.
127 J. Xie, T. Ji, X. Ou-Yang, Z. Xiao and H. Shi, Preparation of $SrTiO_3$ nanomaterial from layered titanate nanotubes, *Solid State Commun.*, 2008, **147**, 226.
128 Y. Li, X. P. Gao, G. R. Li, G. L. Pan, T. Y. Yan and H. Y. Zhu, Titanate Nanofiber Reactivity: Fabrication of $MTiO_3$ (M = Ca, Sr, and Ba) Perovskite Oxides, *J. Phys. Chem. C*, 2009, **113**, 4386.
129 J. Ng, S. Xu, X. Zhang, H. Ying Yang and D. D. Sun, Hybridized Nanowires and Cubes: A Novel Architecture of a Heterojunctioned $TiO_2/SrTiO_3$ Thin Film for Efficient Water Splitting, *Adv. Funct. Mater.*, 2010, **20**, 4287.
130 W. Dong, B. Li, Y. Li, X. Wang, L. An, C. Li, B. Chen, G. Wang and Z. Shi, General Approach to Well-Defined Perovskite $MTiO_3$ (M = Ba, Sr, Ca, and Mg) Nanostructures, *J. Phys. Chem. C*, 2011, **115**, 3918.
131 V. Kalyani, B. S. Vasile, A. Ianculescu, M. T. Buscaglia, V. Buscaglia and P. Nanni, Hydrothermal Synthesis of $SrTiO_3$ Mesocrystals: Single Crystal to Mesocrystal Transformation Induced by Topochemical Reactions, *Cryst. Growth Des.*, 2012, **12**, 4450.
132 K. G. S. Ranmohotti, E. Joseph, J. Choi, J. X. Zhang and J. B. Wiley, Topochemical Manipulation of Perovskites: Low-Temperature Reaction Strategies for Directing Structure and Properties, *Adv. Mater.*, 2011, **23**, 442.
133 S. K. Pradhan, Y. Mao, S. S. Wong, P. Chupas and V. Petkov, Atomic-scale structure of nanosized titania and titanate: particles, wires, and tubes, *Chem. Mater.*, 2007, **19**, 6180.
134 T.-Y. Ma, H. Li, T.-Z. Ren and Z.-Y. Yuan, Mesoporous $SrTiO_3$ nanowires from a template-free hydrothermal process, *RSC Adv.*, 2012, **2**, 2790.
135 J. Yang, J. Zhang, C. Liang, M. Wang, P. Zhao, M. Liu, J. Liu and R. Che, Ultrathin $BaTiO_3$ nanowires with high aspect ratio: a simple one-step hydrothermal synthesis and their strong microwave absorption, *ACS Appl. Mater. Interfaces*, 2013, **5**, 7146.
136 Y. F. Zhu, L. Zhang, T. Natsuki, Y.-Q. Fu and Q.-Q. Ni, Facile synthesis of $BaTiO_3$ nanotubes and their microwave absorption properties, *ACS Appl. Mater. Interfaces*, 2012, **4**, 2101.
137 N. Bao, L. Shen, G. Srinivasan, K. Yanagisawa and A. Gupta, A shape-controlled monocrystalline ferroelectric barium titanate nanostructures: from nanotubes and nanowires to ordered nanostructures, *J. Phys. Chem. C*, 2008, **112**, 8634.
138 F. Maxim, P. M. Vilarinho, P. Ferreira, I. M. Reaney and I. Levin, Kinetic study of the static hydrothermal synthesis of $BaTiO_3$ using titanate nanotubes precursors, *Cryst. Growth Des.*, 2011, **11**, 3358.
139 Y. Xin, J. Jiang, K. Huo, T. Hu and P. K. Chu, Bioactive $SrTiO_3$ nanotube arrays: strontium delivery platform on Ti-based osteoporotic bone implants, *ACS Nano*, 2009, **3**, 3228.
140 J. Zhang, J. H. Bang, C. C. Tang and P. V. Kamat, Tailored TiO_2–$SrTiO_3$ heterostructure nanotube arrays for improved photoelectrochemical performance, *ACS Nano*, 2010, **4**, 387.
141 X. Zhang, K. Huo, L. Hu, Z. Wu and P. K. Chu, Synthesis and photocatalytic activity of highly ordered TiO_2 and $SrTiO_3/TiO_2$ nanotube arrays on Ti substrates, *J. Am. Ceram. Soc.*, 2010, **93**, 2771.
142 Y. Sun, J. W. Liu and Z. H. Li, Design of highly ordered Ag–$SrTiO_3$ nanotube arrays for photocatalytic degradation of methyl orange, *J. Solid State Chem.*, 2011, **184**, 1924.
143 J.-Q. Zheng, Y.-J. Zhu, J.-S. Xu, B.-Q. Lu, C. Qi, F. Chen and J. Wu, Microwave-assisted rapid synthesis and photocatalytic activity of mesoporous Nd-doped $SrTiO_3$ nanospheres and nanoplates, *Mater. Lett.*, 2013, **100**, 62.
144 G. Xu, X. Huang, Y. Zhang, S. Deng, X. Wei, G. Shen and G. Han, Self-assembly and formation mechanism of single crystal $SrTiO_3$ nanosheets via solvothermal route with ethylene glycol as reaction medium, *CrystEngComm*, 2013, **15**, 7206.
145 J. Niu, P.-X. Yan, W.-S. Seo and K. Koumoto, Hydrothermal Synthesis of $SrTiO_3$ Nanoplates Through Epitaxial Self-Assembly of Nanocubes, *J. Nanosci. Nanotechnol.*, 2012, **12**, 2685.
146 T. Cao, Y. Li, C. Wang, C. Shao and Y. Liu, A facile in situ hydrothermal method to $SrTiO_3/TiO_2$ nanofiber heterostructures with high photocatalytic activity, *Langmuir*, 2011, **27**, 2946.
147 H. Bai, J. Juay, Z. Liu, X. Song, S. S. Lee and D. D. Sun, Hierarchical $SrTiO_3/TiO_2$ nanofibers heterostructures with high efficiency in photocatalytic H_2 generation, *Appl. Catal., B*, 2012, **125**, 367.
148 R. Tang and L. Yin, Enhanced photovoltaic performance of dye sensitized solar cells based on Sr-doped $TiO_2/SrTiO_3$ nanorod array heterostructures, *J. Mater. Chem. A*, 2015, **3**, 17417.

149 X. Yue, J. Zhang, F. Yan, X. Wang and F. Huang, An situ hydrothermal synthesis of $SrTiO_3/TiO_2$ heterostructure nanosheets with exposed (0 0 1) facets for enhancing photocatalytic degradation activity, *Appl. Surf. Sci.*, 2014, **319**, 68.

150 M. N. Ha, F. Zhu, Z. Liu, L. Wang, L. Liu, G. Lua and Z. Zhao, Morphology-controlled synthesis of $SrTiO_3/TiO_2$ heterostructures and their photocatalytic performance for water splitting, *RSC Adv.*, 2016, **6**, 21111.

151 J. Luo and P. A. Maggard, Hydrothermal Synthesis and Photocatalytic Activities of $SrTiO_3$-Coated Fe_2O_3 and $BiFeO_3$, *Adv. Mater.*, 2006, **18**, 514.

152 D. Hu, H. Ma, Y. Tanaka, L. Zhao and Q. Feng, Ferroelectric Mesocrystalline $BaTiO_3/SrTiO_3$ Nanocomposites with Enhanced Dielectric and Piezoelectric Responses, *Chem. Mater.*, 2015, **27**, 4983.

153 M. Ye, M. Wang, D. Zheng, N. Zhang, C. Lin and Z. Lin, Garden-like perovskite superstructures with enhanced photocatalytic activity, *Nanoscale*, 2014, **6**, 3576.

154 Z. Zheng, B. Huang, X. Qin, X. Zhang and Y. Dai, Facile synthesis of $SrTiO_3$ hollow microspheres built as assembly of nanocubes and their associated photocatalytic activity, *J. Colloid Interface Sci.*, 2011, **358**, 68.

155 J. O. Eckert, C. C. Hung Houston, B. L. Gersten, M. M. Lencka and R. E. Riman, Kinetics and mechanisms of hydrothermal synthesis of barium titanate, *J. Am. Ceram. Soc.*, 1996, **79**, 2929.

156 R. I. Walton, F. Millange, R. I. Smith, T. C. Hansen and D. O'Hare, Real time observation of the hydrothermal crystallization of barium titanate using in situ neutron powder diffraction, *J. Am. Chem. Soc.*, 2001, **123**, 12547.

157 N. Pienak and W. Bensch, In-situ monitoring of the formation of crystalline solids, *Angew. Chem., Int. Ed.*, 2011, **50**, 2014.

158 Q. Feng, M. Hirasawa and K. Yanagisawa, Synthesis of crystal-axis oriented $BaTiO_3$ and anatase platelike particles by a hydrothermal soft chemical process, *Chem. Mater.*, 2001, **13**, 290.

159 D. Hu, X. Luo, X. Kong, Y. Wang, Y. Tanaka and Q. Feng, Topochemical conversion of protonated titanate single crystals into platelike $Ba_{0.5}Sr_{0.5}TiO_3$ mesocrystals with controllable microstructures, *CrystEngComm*, 2015, **17**, 1758.

160 A. Testino, V. Buscaglia, M. T. Buscaglia, M. Viviani and P. Nanni, Kinetic modeling of aqueous and hydrothermal synthesis of barium titanate ($BaTiO_3$), *Chem. Mater.*, 2005, **17**, 5346.

161 J. Peng, Y. Zhou, H. Wang, H. Zhou and S. Cai, Hydrothermal synthesis and formation mechanism of photocatalytically active $SrTiO_3$ nanocrystals using anatase TiO_2 with different facets as a precursor, *CrystEngComm*, 2015, **17**, 1805.

162 A. Putnis, Why mineral interfaces matter, *Science*, 2014, **343**, 1441.

163 E. Ruiz-Agudo, C. V. Putnis and A. Putnis, Coupled dissolution and precipitation at mineral–fluid interfaces, *Chem. Geol.*, 2014, **383**, 132.

164 P. Cubillas, S. Kohler, M. Prieto, C. Causserand and E. H. Oelkers, How do mineral coatings affect dissolution rates? An experimental study of coupled $CaCO_3$ dissolution—$CdCO_3$ precipitation, *Geochim. Cosmochim. Acta*, 2005, **69**, 5459.

165 F. Xia, J. Brugger, G. Chen, Y. Ngothai, B. O'Neill, A. Putnis and A. Pring, Mechanism and kinetics of pseudomorphic mineral replacement reactions: A case study of the replacement of pentlandite by violarite, *Geochim. Cosmochim. Acta*, 2009, **73**, 1945.

166 A. Kasioptas, T. Geisler, C. Perdikouri, C. Trepmann, N. Gussone and A. Putnis, Polycrystalline apatite synthesized by hydrothermal replacement of calcium carbonates, *Geochim. Cosmochim. Acta*, 2011, **75**, 3486.

167 F. Lucassen, G. Franz, R. Wirth, M. Weise and A. Hertwig, The morphology of the reaction front of the dissolution-precipitation reaction rutile + wollastonite = titanite in time series experiments at 600 °C/400 MPa, *Am. Mineral.*, 2012, **97**, 828.

168 L. Jonas, T. John, H. E. King, T. Geisler and A. Putnis, The role of grain boundaries and transient porosity in rocks as fluid pathways for reaction front propagation, *Earth Planet. Sci. Lett.*, 2014, **386**, 64.

169 J. Zhao, J. Brugger, Y. Ngothai and A. Pring, The replacement of chalcopyrite by bornite under hydrothermal conditions, *Am. Mineral.*, 2014, **99**, 2389.

170 Y. Zhang, L. Zhong and D. Duan, A single-step direct hydrothermal synthesis of $SrTiO_3$ nanoparticles from crystalline P25 TiO_2 powders, *J. Mater. Sci.*, 2016, **51**, 1142.

171 W. Sun, Y. Pang, J. Li and W. Ao, Particle Coarsening II: Growth Kinetics of Hydrothermal $BaTiO_3$, *Chem. Mater.*, 2007, **19**, 1772.

172 J. Yang, B. Geng, Y. Ye and X. Yu, Stick-like titania precursor route to $MTiO_3$ (M = Sr, Ba, and Ca) polyhedral, *CrystEngComm*, 2012, **14**, 2959.

173 D. Spagnoli, J. F. Banfield and S. C. Parker, Free-energy change of aggregation of nanoparticles, *J. Phys. Chem. C*, 2008, **112**, 14731.

174 M. L. Moreira, V. M. Longo, W. Avansi Jr, M. M. Ferrer, J. Andrés, V. R. Mastelaro, J. A. Varela and É. Longo, Quantum Mechanics Insight into the Microwave Nucleation of $SrTiO_3$ Nanospheres, *J. Phys. Chem. C*, 2012, **116**, 24792.

175 L. F. da Silva, W. Avansi Jr, J. Andres, C. Ribeiro, M. L. Moreira, E. Longo and V. R. Mastelaro, Long-range and short-range structures of cube-like shape $SrTiO_3$ powders: microwave-assisted hydrothermal synthesis and photocatalytic activity, *Phys. Chem. Chem. Phys.*, 2013, **15**, 12386.

176 T. Setinc, M. Spreitzer, D. Vengust, I. Jerman and D. Suvorov, Inherent defects in sol-precipitation/hydrothermally derived $SrTiO_3$ nanopowders, *Ceram. Int.*, 2013, **39**, 6727.

177 H. Zhan, Z.-G. Chen, J. Zhuang, X. Yang, Q. Wu, X. Jiang, C. Liang, M. Wu and J. Zou, Correlation between Multiple Growth Stages and Photocatalysis of $SrTiO_3$ Nanocrystals, *J. Phys. Chem. C*, 2015, **119**, 3530.

178 H. Xu, S. Quan Wei, H. Wang, M. K. Zhu, R. Yu and H. Yan, Preparation of shape controlled $SrTiO_3$ crystallites by sol–gel-hydrothermal method, *J. Cryst. Growth*, 2006, **292**, 159.

179 Y. Wang, G. Xu, L. Yang, Z. Ren, X. Wei, W. Weng, P. Du, G. Shen and G. Han, Formation of single-crystal $SrTiO_3$ dendritic nanostructures via a simple hydrothermal method, *J. Cryst. Growth*, 2009, **311**, 2519.

180 Q.-S. Wu, J.-W. Liu, S.-F. Chen, H.-W. Liang and S.-H. Yu, Surfactant-free synthesis of $SrTiO_3$ hierarchical structures in ethanol/water mixed solvent at room temperature, *CrystEngComm*, 2015, **17**, 6895.

181 S. I. Suárez-Váquez, S. Gil, J. M. García-Vargas, A. Cruz-López and A. Giroir-Fendler, Catalytic oxidation of toluene by $SrTi_{1-x}B_xO_3$ (B = Cu and Mn) with dendritic morphology synthesized by one pot hydrothermal route, *Appl. Catal., B*, 2017, DOI: 10.1016/j.apcatb.2017.04.042.

182 K. D. Kreuer, Proton-conducting oxides, *Annu. Rev. Mater. Res.*, 2003, **33**, 333.

183 N. Sata, K. Hiramoto, M. Ishigame, S. Hosoya, N. Niimura and S. Shin, Site identification of protons in $SrTiO_3$: Mechanism for large protonic conduction, *Phys. Rev. B: Condens. Matter Mater. Phys.*, 1996, **54**, 15795.

184 D. Hennings and S. Schreinemacher, Characterization of Hydrothermal Barium Titanate, *J. Eur. Ceram. Soc.*, 1992, **9**, 41.

185 D. F. K. Hennings, C. Metzmacher and B. S. Schreinemacher, Defect chemistry and microstructure of hydrothermal barium titanate, *J. Am. Ceram. Soc.*, 2001, **84**, 179.

186 E.-W. Shi, C.-T. Xia, W.-Z. Zhong, B.-G. Wang and C.-D. Feng, Crystallographic properties of hydrothermal barium titanate crystallites, *J. Am. Ceram. Soc.*, 1997, **80**, 1567.

187 G. Busca, V. Buscaglia, M. Leoni and P. Nanni, Solid-State and Surface Spectroscopic Characterization of $BaTiO_3$ Fine Powders, *Chem. Mater.*, 1994, **6**, 955.

188 T. Noma, S. Wada, M. Yano and T. Suzuki, Analysis of lattice vibration in fine particles of barium titanate single crystal including the lattice hydroxyl group, *J. Appl. Phys.*, 1996, **80**, 5223.

189 M. Viviani, M. T. Buscaglia, A. Testino, V. Buscaglia, P. Bowen and P. Nanni, The influence of concentration on the formation of $BaTiO_3$ by direct reaction of $TiCl_4$ with $Ba(OH)_2$ in aqueous solution, *J. Eur. Ceram. Soc.*, 2003, **23**, 1383.

190 E. Ciftci, M. N. Rahaman and M. J. Shumsky, Hydrothermal precipitation and characterization of nanocrystalline $BaTiO_3$ particles, *Mater. Sci.*, 2001, **36**, 4875.

191 M. L. Moreira, V. M. Longo, W. Avansi, Jr., M. M. Ferrer, J. Andrés, V. R. Mastelaro, J. A. Varela and É. Longo, Quantum Mechanics Insight into the Microwave Nucleation of $SrTiO_3$, *J. Phys. Chem. C*, 2012, **116**, 24792.

192 F. A. Rabuffetti, H.-S. Kim, J. A. Enterkin, Y. Wang, C. H. Lanier, L. D. Marks, K. R. Poeppelmeier and P. C. Stair, Synthesis-Dependent First-Order Raman Scattering in $SrTiO_3$, *Chem. Mater.*, 2008, **20**, 5628.

193 S. Fuentes, R. A. Zarate, E. Chavez, P. Munöz, D. Diaz-Droguett and P. Leyton, Preparation of $SrTiO_3$ nanomaterial by a sol–gel-hydrothermal method, *J. Mater. Sci.*, 2010, **45**, 1448.

194 H. Nakano, K. Urabe, T. Oikawa and H. Ikawa, Characterization of internal pores in hydrothermally synthesized $BaTiO_3$ particle by Transmission Electron Microscopy, *J. Am. Ceram. Soc.*, 2004, **87**, 1594.